



Systematic studies on blood coagulation mechanisms of halloysite nanotubes-coated PET dressing as superior topical hemostatic agent

Yue Feng^a, Xiang Luo^b, Fan Wu^a, Hongzhong Liu^a, Enyu Liang^c, Rong-Rong He^{b,*}, Mingxian Liu^{a,*}

^a Department of Materials Science and Engineering, Jinan University, Guangzhou 510632, China

^b College of Pharmacy, Jinan University, Guangzhou 510632, China

^c Department of Laboratory Medicine, the Second Affiliated Hospital of Guangzhou University of Chinese Medicine, Guangzhou, 510120, China

ARTICLE INFO

Keywords:

Clay nanotube
Coagulation
Platelet activation
Hemostasis
Biocompatibility

ABSTRACT

Halloysite nanotubes (HNTs), a traditional mineral Chinese medicine, have been used to stop bleeding for thousands of years. However, the coagulation mechanisms of HNTs and their practical application potential have not been fully elucidated. In this study, HNTs were found to accelerate hemostasis via multiple dependent approaches: (i) absorbing water and concentrating blood due to their super-hydrophilicity and unique tubular nanostructure; (ii) triggering an intrinsic coagulation cascade by negatively charged surface interaction; and (iii) accelerating clot formation by activating and linking with platelets. To solve the difficulty in the application of powder, a HNT-coated polyester fiber dressing was designed by an impregnation method. The HNT coating enables the dressing to resist massive hemorrhaging of the liver and vessels, as well as epidermal bleeding. Moreover, the HNT-coated fiber dressings are not accompanied by burning or adhesion at the wound sites. In summary, this work provides profound insight into HNT hemostasis through the physical and biological interactions between HNTs and blood, which represents a promising strategy for effective prehospital treatment and civilian needs.

1. Introduction

Unnecessary bleeding caused by trauma, surgery, and coagulopathy contributes to the majority of deaths on the battlefield and daily life [1]. A few types of hemostatic materials including polysaccharides, [2,3] silicates, [4] biological products, [5] and nano-self-assembled peptides, [6] have been developed to accelerate coagulation. Among these, silicate hemostats, including zeolite, kaolin, and Montmorillonite (MMT), have become popular owing to their high efficiency, manipulability, cost-effectiveness, and minimal tissue reactivity [7]. Silicate hemostats usually operate through three different mechanisms: (i) absorbing water highly efficiently, resulting in blood concentration (zeolites); (ii) activating Hageman factor XII (FXII) to initiate the intrinsic coagulation pathway, in which FXII binds to a negatively charged surface via positively charged amino acids in its heavy chain (kaolin and diatomite); [8,9] and (iii) forming a physical barrier to block blood flow (MMT). Animal and clinical trials have shown that clay-based hemostats are superior to zeolite because they can stop bleeding without heat, thus

avoiding burns.

However, commercial clay hemostats still present challenges. WoundStat® based on MMT swells with fluid, resulting in difficulty in debridement and inflammation; [10] QuikClot® Combat Gauze (CG), a kaolin-impregnated dressing, has been the only hemostatic dressing used by the US military since 2008, [11] however, the restricted surface area and insufficient cation exchange [12] of kaolin lead to the suboptimal hemostatic effect of CG, which might not be suitable for cases of coagulopathy [13]. In recent years, great progress has been made in the development of novel clay hemostatic materials. For example, Long et al. developed a kaolin/ α -Fe₂O₃ composite for effective and rapid hemostasis via activating Red blood cells (RBCs) aggregation [14]. The flexible zeolite-cotton hybrid hemostat prepared by the on-site template-free growth method exhibited higher procoagulant activity, minimized the loss of active components, and demonstrated better scalability for practical applications [15].

Halloysite, with the trade name Chishizhi, is a traditional mineral hemostatic medicine that has been used in China to stop bleeding for

* Corresponding authors.

E-mail addresses: rongronghe@jnu.edu.cn (R.-R. He), liumx@jnu.edu.cn (M. Liu).

<https://doi.org/10.1016/j.cej.2021.132049>

Received 16 June 2021; Received in revised form 13 August 2021; Accepted 22 August 2021

Available online 26 August 2021

1385-8947/© 2021 Elsevier B.V. All rights reserved.

thousands of years. Microscopically, halloysite shows a perfect tubular morphology with an empty lumen. Chemically, Halloysite nanotubes (HNTs) have the molecular formula $\text{Al}_2\text{Si}_2\text{O}_5(\text{OH})_4 \cdot n\text{H}_2\text{O}$. It is unclear whether a relationship exists between hemostatic properties and the structure and/or chemical composition of HNTs. HNTs share a similar chemical structure to kaolin but roll into a hollow tube with a diameter of approximately 50 nm and length of approximately 1000 nm. The tubular morphology endows HNTs with a negative Si–O–Si external surface and a positive Al–OH internal surface. Compared with platy kaolin multilayer stacks, [16] the unique tubular structure and high aspect ratio of HNTs provide higher surface area, pore volume, and Cation exchange capacity (CEC), [17] implying higher hemostasis potential. Previous studies have reported that the doping of HNTs can enhance the hemostatic effect of materials. For instance, our work demonstrated that the addition of 67% HNTs to a chitosan sponge resulted in an 89% increase in clotting ability [18]. Likewise, Alavi et al. reported that bentonite-HNT-impregnated gauze significantly decreased clotting time in a rat model [19]. Udangawa et al. also found that the average plasma coagulation time of HNTs was 55 s, which is faster than that of kaolin, confirming that HNTs were superior to kaolin in hemostasis [20]. As an economically feasible and biocompatible clay material, HNTs show promising potential in multiple biomedical areas such as drug delivery, wound healing, and bone regeneration [21]. Several reports have demonstrated the high biocompatibility and biosafety of HNTs [22,23]. A comparative study on *paramecium caudatum* protozoans confirmed that HNTs were more biocompatible than other nanoclays (MMT, bentonite, and kaolin) [22]. Cytotoxicity assays showed that HNTs were nontoxic to human umbilical vein endothelial cells. [23,24] In addition, polymer/HNT composite tissue engineering scaffolds in rats exhibited excellent hemocompatibility, [25] and a blood compatibility study on rabbit blood reported a hemolysis ratio of less than 0.5% when treated with HNTs, indicating the non-hemolytic property of HNTs [26]. Therefore, compared with other silicate hemostatic materials, HNTs are expected to be more promising owing to their higher biocompatibility and safety.

Although the improved hemostatic effect of HNTs has been observed in previous studies, [18,19,20] the underlying coagulation mechanisms and practical application forms of HNTs have not been fully elucidated. In this study, we explored the coagulation mechanisms of HNTs and designed an HNT-coated Polyethylene terephthalate (PET) fiber dressing (HNTs-PET) that exhibits superior hemostatic activity and safety in in-vitro and in-vivo rat experiments.

2. Experimental section

2.1. Materials

Purified HNTs were obtained from Guangzhou Runwo Materials Technology Co., Ltd., China. PET fiber dressings were produced by Johnson and Johnson (USA). QuikClot Combat Gauze was obtained from Chinook Medical Gear, Inc., USA. Zeolite, kaolin, MMT, calcium chloride, paraformaldehyde, and glutaraldehyde were purchased from Shanghai Macklin Biochemical Co., Ltd., China.

The Activated partial thromboplastin time (APTT) kit was purchased from Beijing Leagene Biotechnology Co., Ltd., China. FITC anti-rat CD41 and PE anti-rat CD62p antibodies were purchased from Beijing 4A Biotech Co., Ltd. (China), and BD Biosciences (USA), respectively. Tirofiban was purchased from Selleck Chemicals (Houston, TX, USA). Collagen I was acquired from BioFroxx (Germany), and isoflurane was obtained from the RWD (China). Depilatory cream was purchased from Veet (France).

Citrated sheep whole blood (1:9 ratio of sodium citrate to blood) was acquired from Shanghai Yuduo Biological Technology Co., Ltd., China, and the L929 cell line was purchased from the American Type Culture Collection (USA). The animals were ordered from the Guangdong Pharmaceutical University Undergraduate Laboratory Animal Center,

China.

All cell culture reagents were ordered from Thermo Fisher Scientific (USA). Acridine orange/Ethidium bromide (AO/EB) staining solution was purchased from Beijing Solarbio Science & Technology Co., Ltd., China. Cell Counting Kit-8 (CCK-8) reagents were acquired from Dojindo Laboratories (Japan). Ultrapure water was prepared using a Milli-Q Integral Water Purification System (Germany).

2.2. Preparation of HNTs-PET

An aqueous dispersion of HNTs was freshly prepared and briefly homogenized by ultrasound (output frequency 40 kHz, 10 min, and 30 W) before use. Then, the PET fiber dressing was immersed in the HNT dispersion, ultrasonically treated for 1 h, and dried at 60 °C for 8 h. Before their biological performance was assessed, the fiber materials were sterilized using ultraviolet radiation or moist-heat sterilization.

2.3. Characterization of HNTs and HNTs-PET

For Transmission electron microscopy (TEM), Atomic force microscopy (AFM), particle size distribution analysis, and zeta potential assay of the HNT samples, an aqueous dispersion of HNTs (0.05 wt%) was prepared. The morphologies were observed using a TEM instrument (JEM, 1400 Flash) at 100 kV and AFM instrument with a contacting model (BioScope Catalyst NanoScope V, Bruker Instruments Ltd., USA). The particle size distribution and zeta potential were analyzed using a Nano ZS zeta potential analyzer (Malvern Instruments Co., U.K.).

The surface morphology of HNTs-PET was observed using a Field emission scanning electron microscope (FE-SEM) (ULTRA55, Carl Zeiss Jena Co. Ltd., Germany) after sputter-coating with gold with a thickness of 5 nm. Polarized microscopy (POM) photographs of the fibers were taken using a BX51 microscope (Olympus, Japan). The X-ray diffraction (XRD) patterns were recorded on a Miniflex 600 diffractometer (Rigaku Corporation, Japan) at 40 kV with a current of 40 mA. Fourier-transform infrared (FTIR) spectra were obtained by attenuated total reflectance using a Thermo Fisher spectrometer (Nicolet iS50, Thermo Fisher Scientific Co. Ltd., USA). The thermal stability of the materials was analyzed using Thermogravimetric analysis (TGA) on a TGA2 instrument (Mettler Toledo, Co. Ltd., Switzerland).

2.4. Surface wettability and absorption property evaluation

The HNT tablets (1 g of clay powder) were prepared using a universal pressing machine at a pressure of 10 MPa to avoid the capillarity interference of the uneven tablet surface. To measure the contact angle and blood absorption time, a 20 μL droplet (ultrapure water or blood) was delivered onto the tablets. The contact angles were measured using a DSA-100 goniometer (Kruss Co., Ltd., Germany). Videos were recorded from 0 min until the contact angles were less than 10°, and photographs of clots generated on the HNT tablets were taken.

2.5. Water absorption capacity

An appropriate amount of clay powder was placed into a clean glass dish and weighed, and then water was added until the powder was fully saturated. Three tests were conducted for each group; the results are presented as mean \pm Standard deviation (SD). The water absorption ratio was calculated as follows:

$$\text{Water absorption ratio (\%)} = \frac{\text{weight}_{\text{water}}}{\text{weight}_{\text{material}}} \times 100\%$$

2.6. Whole blood clotting time assay

The coagulation ability of different mineral materials was evaluated. All subsequent processes were performed in Eppendorf tubes at 37 °C.

After preheating, a 1 mL volume of sodium-citrated sheep blood was mixed with 1 mg of zeolite, MMT, kaolin, or 0, 1, 2, 4, 8, or 16 mg of HNT powder. Later, the test tubes were incubated in a water bath at 37 °C for 5 min. A recalcification reagent (0.2 M CaCl₂) was added to tubes in a volume ratio of 1:10 to initiate coagulation. The progress of clotting was observed by shaking and tilting the tubes every 10 s. The duration was recorded as clotting time until the blood was completely coagulated. To select an optimum HNT coating, several HNTs-PET samples (ranging from 0.05% to 2%, 1 mg mL⁻¹ blood in each tube, and 1 mg HNT powder as a positive control) were tested.

A 200 µL volume of blood (CaCl₂ was added to initiate coagulation) was immediately added between the two pieces of dressing in a Petri dish. The samples were kept at 37 °C clotting for 0, 3, 6, and 9 min, and then 10 mL of ultrapure water was gently added to terminate the reactions without disturbing the clots. Free RBCs (instead of blood cells agglomerated by fibrin clots) hemolyzed and released hemoglobin (HA) into the water. Blood (200 µL) was directly added to an empty Petri dish as a blank control. The absorbance of HA(*t*) was measured at 540 nm using a spectrophotometer at different time points. The absorbance HA(*t*) reflects the hemoglobin released by the free RBCs. HA(0) is the absorbance at 0 min, representing the uncoagulated state, which was used as a reference. All experiments were repeated thrice. The relative hemoglobin absorbance (RHA) was calculated as follows:

$$RHA (\%) = \frac{HA(t)}{HA(0)} \times 100\%$$

2.7. Intrinsic coagulation cascade activation assay

The APTT assay is a monitor of the intrinsic coagulation system, which usually uses kaolin as a pathway activator [27,28]. A modified manual APTT method was used to test the intrinsic coagulation cascade activation. In citrated Platelet poor plasma (PPP), the addition of a platelet substitute, FXII activator (generally kaolin, micronized silica, etc.) and CaCl₂ will allow fibrin clot formation. Here, HNTs or kaolin (as a positive control) were used as the contact activator of FXII to replace the original activator in the commercial APTT kit.

First, fresh blood was centrifuged at 3000 rpm for 10 min to obtain PPP. Before testing, all reagents and plasma were preheated to 37 °C to compare the activation effect; HNTs or kaolin (final concentration: 1 mg mL⁻¹) and phospholipids were mixed and incubated within 1 mL of PPP at 37 °C. A CaCl₂ solution (25 mM) was added in a volume ratio of 1:1 to initiate clotting. The fibrin clot formation time was obtained via APTT, where a shorter APTT signified more efficient contact activation of the intrinsic coagulation cascade. Experiments were performed using three different blood samples.

2.8. Clinical standard blood coagulation tests

Clinical APTT, Prothrombin time (PT), Thrombin time (TT), and Fibrinogen (FIB) tests were conducted using an automatic coagulation analyzer (RAC-030, Rayto, China). PPP (500 µL) was treated with HNTs (final concentration: 1, 2, or 4 mg mL⁻¹) or kaolin (final concentration: 1 mg mL⁻¹) at 37 °C for 5 min and measured using an automatic coagulation analyzer.

2.9. Platelet activation and aggregation analysis

For FE-SEM analysis of platelets, fresh whole blood was centrifuged at 150 × g at room temperature for 10 min to obtain platelet rich plasma. A platelet diluent was prepared to reduce the interference of plasma proteins, and the diluent was incubated at 37 °C. The interaction of HNTs with platelets was evaluated by mixing 450 µL of platelet solution with 50 µL of HNT suspension (final concentration: 1 mg mL⁻¹). The mixture was incubated at 37 °C for 15 min and fixed with 4% paraformaldehyde for 30 min. Then, the mixture was smeared on a glass slide

and washed twice with Phosphate-buffered saline (PBS). Glutaraldehyde (2.5%) was used for secondary cell fixation and washed with PBS. The samples were dehydrated in an ethanol series and vacuum-dried. After sputter-coating with a thin film of gold, the samples were observed by FE-SEM.

To quantify platelet activation, fresh citrated whole blood was obtained for the flow cytometry (FCM) assay. A 10 µL volume of test solution (HNTs dispersed in PBS at 1 mg mL⁻¹, 10 mM of collagen solution as the positive control, or 1 mM of tirofiban as operating fluid) was mixed with 90 µL of whole blood for 5 min. Tirofiban, a glycoprotein IIb/IIIa (GPIIb/IIIa) complex inhibitor, was used for the reversal experiment [29,30]. Next, 5 µL of treated blood was stained with platelet-activation-dependent monoclonal antibodies (FITC anti-rat CD41 for platelet activation, PE anti-rat CD62p for activation identification) [30]. Finally, a flow cytometer (Canto II, BD Biosciences, USA) was employed to analyze the data using FlowJo 10.0.2 software (BD Biosciences, USA). Experiments were performed on three different blood samples.

2.10. In vitro vascular injury model hemostasis assay

An opening (7 mm × 7 mm) was made on a polyethylene hose (mimicking the vascular tissue) to simulate the wound (internal diameter: 10 mm), which was sealed with the HNTs-PET and PET using medical tape. The entire blood vessel model was fixed on a pre-weighed Petri dish. Blood (mixed with CaCl₂ to restart clotting) was added to the hose (3 mL of each). After removing the hose, the weight gain of the Petri dish reflected blood loss in this vascular model. The duration from the beginning to the end of the blood exudation was the hemostatic time. The results were averaged over three repetitions (n = 3).

2.11. Animals

Pathogen-free Sprague–Dawley rats (male, 8–10 weeks old, ≈250 g) were obtained from Guangdong Pharmaceutical University Undergraduate Laboratory Animal Center (Guangzhou, China) with approval from the Institutional Animal Care and Use Committee (IACUC) of Jinan University (approval number: 20200319–32). All animals were fasted for 24 h before the experiments. Rats were anesthetized with isoflurane (4% for induction and 2% for maintenance) using a multi-channel animal anesthesia machine (R550, RWD, China) with a heating blanket to avoid bleeding-induced hypothermia. All rats were euthanized by excessive anesthesia.

2.12. In vivo hemostatic capability and adhesion evaluation

In vivo hemostasis evaluations were performed using rat liver and femoral arteriovenous injury models. In the model of liver injury (n = 4), the rats were anesthetized and exposed to the middle lobe of the liver. Several sheets of filter paper were placed underneath the liver for accurate statistics of blood loss. An incision (length: 1.0 cm; depth: 0.5 cm) was made in the middle lobe of the liver to cut off the hepatic venous plexus, which resulted in severe bleeding [31,32]. Instantly after injury, the HNTs-PET, PET, and CG dressings were applied on incisions with pressing and timing. Blood loss was characterized by measuring the weight increase of the dressings and filter paper. For the exothermic reaction, an infrared thermometer was used to monitor the wound temperature.

For the femoral arteriovenous injury model (n = 4), the rat hair in the surgical area was removed cleanly. The inner skin thigh was carved and exposed to femoral vessels. Severe hemorrhage was created by transecting the femoral vascular bundle. HNTs-PET, PET, and CG dressings were applied to the wounds instantly, and hemostasis time, blood loss, and wound temperature were recorded.

The tangential wound model was enacted on the back of the rat (n = 4). The hair was completely removed to prevent interference during the

adhesion test. A window (15 × 7 mm) was made in the middle of transparent medical tape (40 × 30 mm) for blood penetration observation, and the test dressing (25 × 15 mm) was fixed in the tapes. Incisions (length: 1 cm, deep into the muscle) on the left and right sides of the back were created. HNTs-PET and PET were immediately applied, and photographs were taken. At 3 min, the wounds were examined, and the blood-soaked dressing was weighed for blood loss. Next, the peak peel forces were tested using a tension meter (range: 1000 mN, accuracy: 0.01 mN) for adhesion evaluation.

2.13. Cytotoxicity

The cytotoxicity of HNTs-PET was assessed using the mouse fibroblast cell line L929, which is commonly used for cytotoxicity assays of wound dressings [33,34]. The cells were cultured in minimum essential medium supplemented with 10% fetal bovine serum and 1% penicillin–streptomycin solution in 5% CO₂ at 37 °C.

Morphological evidence of cell viability was analyzed using AO/EB staining. Autoclaved HNTs-PET were soaked in complete medium overnight to obtain 100% leachate (every 10 mg in 1 mL medium). A gradient-proportional soaking medium of HNTs-PET was prepared, which contained 0% and 20, 40, 60, 80, or 100% material leachate. L929 cells (3 × 10⁴ mL⁻¹) were inoculated in 24-well plates, cultured overnight, and treated with leachates for 24 or 48 h. Cell morphology was recorded using a fluorescence microscope (XDY-2, Guangzhou Liss Optical 731 Instrument Ltd., China) after AO/EB staining.

The Cell Counting Kit-8 assay was used for the cytotoxic assay. L929 cells (3 × 10⁴ mL⁻¹) in the logarithmic growth phase were inoculated in a 96-well plate (100 μL/well) and treated with HNTs-PET leachate. After 24 or 48 h, 10 μL of CCK-8 solution was added to each well and incubated for 2 h at 37 °C. Finally, the absorbance was measured at 450 nm using a microplate reader (Elx800, BioTek, USA). The results are reported as mean ± SD (n = 4).

2.14. Blood compatibility

Sodium citrated sheep whole blood (1 mL) was added to 10 mL of PBS and centrifuged at 500 × g for 10 min three times to collect RBCs from the blood. Diluted RBCs (200 μL) were added to 800 μL of the sample suspension (from 37.5 to 1200 μg mL⁻¹). The sample suspension was prepared using HNTs-PET fragments (cut into pieces) mixed with PBS. Ultrapure water (+RBCs) and PBS (+RBCs) was used as positive and blank controls, respectively. All samples were incubated at 37 °C for 2 h. Then, the samples were centrifuged at 1000 × g for 5 min to precipitate RBCs. The absorbance at 540 nm was measured using a microplate reader (Elx800, BioTek, USA). The hemolysis rate was calculated as follows:

$$\text{Hemolysis rate (\%)} = \frac{OD_{\text{sample}} - OD_{\text{blank}}}{OD_{\text{positive}} - OD_{\text{blank}}} \times 100\%$$

2.15. Skin irritation test

Rat back skin was used for the irritation test of HNTs-PET. The HNTs-PET and PET were covered on the back skin for 24 h to observe erythema, itching, or cracking. Subsequently, the skin (10 × 10 mm) in the test areas was sampled and fixed in 4% paraformaldehyde for 2 days. After paraffin embedding and slicing, Hematoxylin and Eosin (H&E) staining was conducted at Wuhan Servicebio Biotechnology Co., Ltd., China. Representative images were obtained using a microscope (BX51, Olympus, Japan).

2.16. Statistical analysis

The data are presented as the mean ± SD. Statistical comparisons of the data were conducted using GraphPad Prism 7 (GraphPad Software,

USA). The between-group differences were analyzed using a one-way analysis of variance (ANOVA). Differences were considered statistically significant at $p < 0.05$.

3. Results

3.1. Hemostatic potential of HNTs

HNTs are natural clay materials formed by rolling aluminosilicate kaolin sheets 15–40 times, and this process endows HNTs with special characteristics with external negatively charged Si–O–Si surfaces and inner positively charged Al–OH surfaces (Fig. 1a). The TEM (Fig. 1a), SEM, and AFM (Fig. S1a and S1b) images show that the HNTs exhibit a tubule-like morphology with an empty lumen and high aspect ratio. The total negative charge of HNTs is approximately -51.6 ± 1.6 mV at pH 7.2, which results in repulsive forces among the tubes and good dispersion in water (Fig. S1c and S1d) [35].

Halloysites with excellent procoagulant potential have been recognized for thousands of years. However, the blood clotting laws of HNTs and their related mechanisms remain unclear. Hence, we compared whole blood clotting of HNTs with other aluminosilicate hemostatic materials. The coagulation efficiency of HNTs lies between that of zeolite and MMT and is about 2.3-fold faster than kaolin (Fig. 1b). HNTs at a low concentration of 1 mg mL⁻¹ are sufficient to accelerate blood coagulation, which is approximately three-fold that of the natural process and is concentration-dependent in vitro (Fig. 1c). The clotting time gradually decreased from 70 to 55 s as the HNT concentration increased.

Aluminosilicate hemostats such as zeolites possess the ability to absorb water, which concentrate blood components in the bleeding site [36]. The wettability and absorption capacity of HNTs toward water and blood were assessed using the dynamic contact angle. The results show that HNTs are super-hydrophilic with rapid water absorption (within 10 s, $\theta = 0^\circ$). The contact angle of blood on the HNT cake was 43.4° upon contact and then quickly decreased to 8.9° after 10 min (Fig. 1d, e). As the blood contact angle slowly decreased, blood clotted spontaneously despite being anticoagulated with sodium citrate. As shown in Fig. 1f, the water droplet was completely absorbed within 5 s. Blood droplets are gradually concentrated and form black clots, which then dry due to severe dehydration, forming a fragile plate. The blood clot, together with a thin HNT layer, can be easily peeled off (Fig. 1f, right). Thus, HNTs can absorb water from whole blood to trigger natural blood coagulation. To investigate the relationship between water absorption capacity and blood clotting ability, the water absorption ratio of other hemostatic minerals was measured. The absorption ratio of HNTs was found to be close to that of zeolite (approximately 80% of its own volume), which is significantly higher than that of MMT and kaolin (Fig. S2a). Therefore, the factor concentration effect of HNTs by water absorption plays a critical role in its excellent procoagulant effect.

3.2. Intrinsic coagulation pathway and platelet activation of HNTs

The intrinsic coagulation pathway is often activated by blood contacting negatively charged surfaces, which is also known as the “glass effect” [37]. To verify whether HNTs have this effect, a modified APTT test using HNTs or kaolin (as a positive control) as a pathway activator was performed. HNTs (17 ± 3 s) shortened the APTT to half that of the blank group (39 ± 4 s), making HNTs significantly more efficient than kaolin (26 ± 5 s) (Fig. 2a). The zeta potential of several clay hemostatic materials showed that HNTs are the most negatively charged among them, at approximately -51.6 ± 1.6 mV (Fig. 2b). These data confirm the more effective FXII self-activation pathway of HNTs, which is beneficial for acute intrinsic coagulation cascade triggering. Clinical standard coagulation tests were also carried out to evaluate the impact of HNTs on extrinsic coagulation cascade activation and plasma fibrin formation speed (Fig. S3). No significant difference was found between the kaolin group and blank control group, nor between the HNTs group

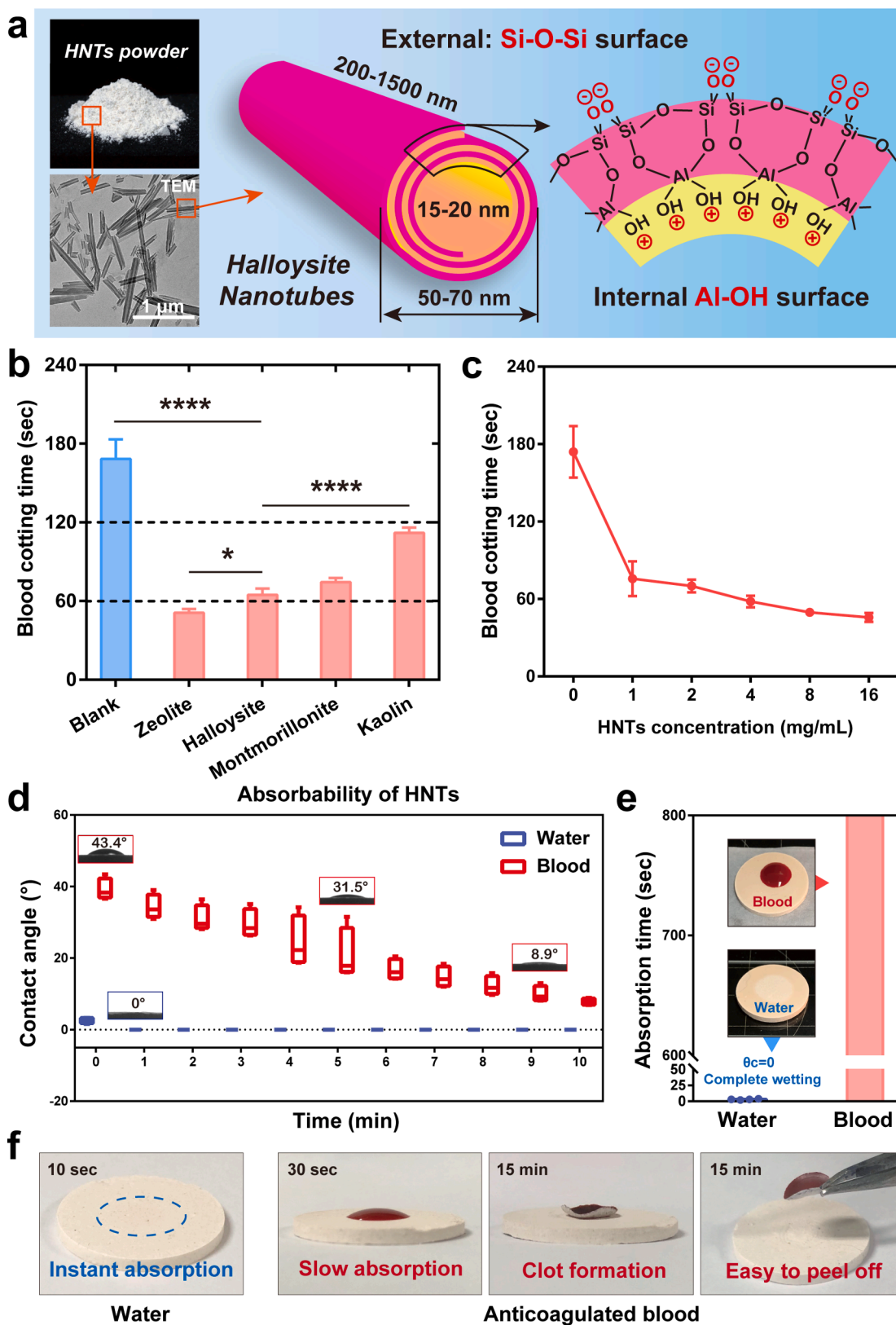


Fig. 1. Characterization of HNTs and their rapid coagulation ability. (a) Appearance of HNTs powder, TEM image, and schematic diagram of HNTs' tubular structure and molecular structure. (b) Clotting times of HNTs compared to those of other inorganic hemostatic materials (n = 3). (c) Blood clotting time of HNTs with different concentrations (n = 3). (d) Contact angle of HNT powder to water or blood. (e) Water and blood absorption times of HNTs. (f) Representative photographs of HNT surface wettability with water and blood. Data values correspond to mean ± SD. Error bars represent SD. ****p < 0.0001, *p < 0.05, one-way Analysis of variance (ANOVA).

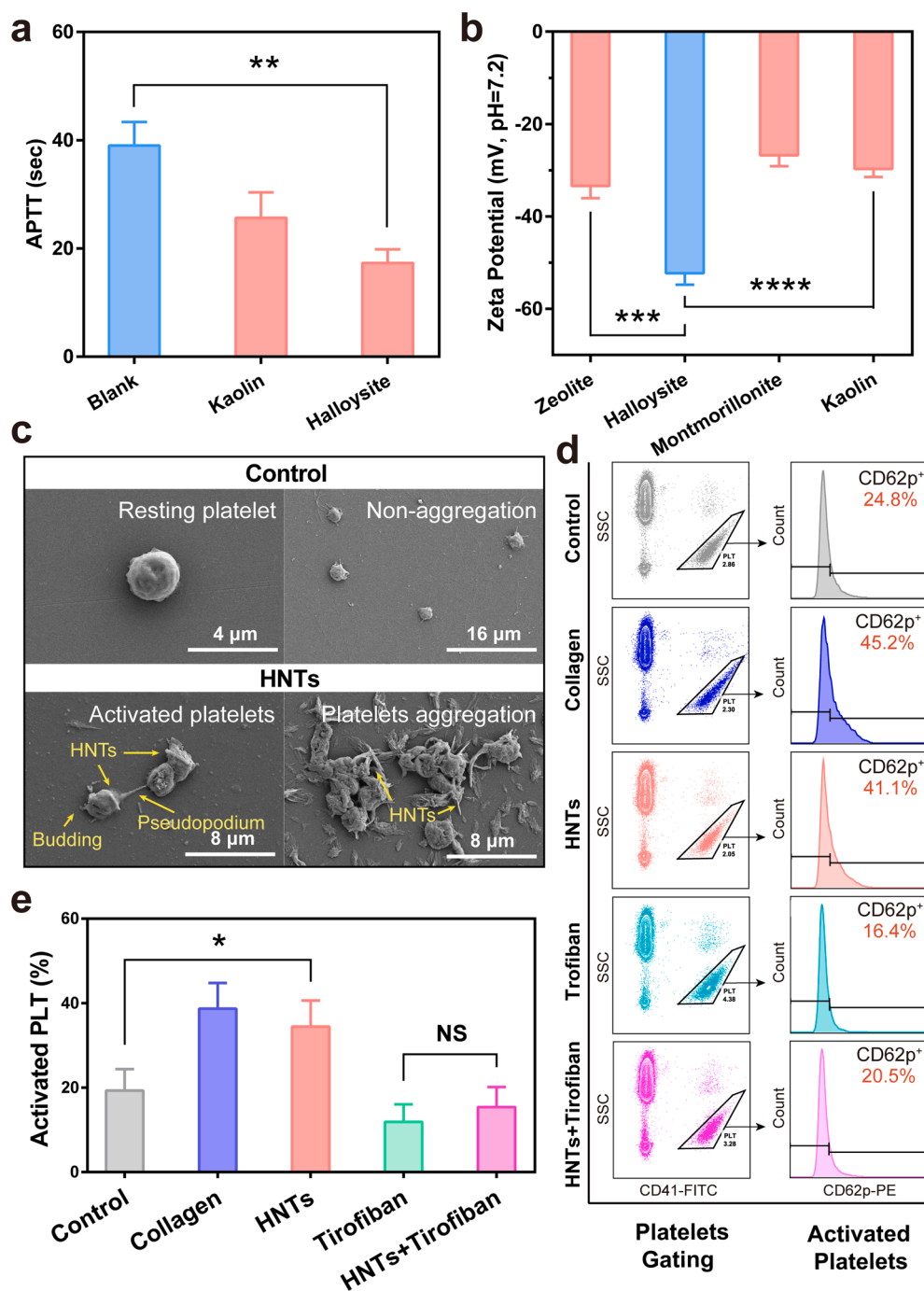


Fig. 2. Intrinsic coagulation pathway activation and platelets interaction of HNTs. (a) The APTT results. (b) Zeta potential of HNTs and other inorganic hemostatic materials. (c) FE-SEM images of resting and non-aggregated platelets of the control, and the activated and aggregated platelets cross-linked with HNTs. (d) FCM analysis diagram of platelet activation (CD41⁺CD62p⁺) of HNTs, fresh blood without treatment (control), collagen (positive control), and tirofiban (reversion) (n = 3). (e) Statistical graph of platelet activation rates relative to the FCM analysis (n = 3). (**p* < 0.05, ***p* < 0.01, ****P* < 0.001, *****P* < 0.0001. Data are analyzed by one-way ANOVA, and expressed as mean \pm SD).

and control group.

Several modification strategies have been employed to alter the surface properties of HNTs, such as enhancing negative charges or establishing positive charges. Surprisingly, charge conversion did not affect the whole blood clotting time of the HNTs (Fig. S2b), implying the existence of non-factor-dependent pathways. Unlike the platelet poor plasma used in the APTT assay, the whole blood clotting assay is more complicated and includes the participation of platelets. Based on these results, the interaction between platelets and HNTs was detected. As shown in Fig. 2c, the FE-SEM images of platelet morphology revealed a smooth surface and dispersed distribution of platelets with discoid shape in the control group. In contrast, HNTs significantly induced platelet activation, as evidenced by pseudopodia formation, membrane budding, and aggregation. As displayed in the FCM graphs (Fig. 2d and 2e), the

statistics indicated that the proportion of activated platelets (CD41⁺CD62p⁺ cells) in the total number of platelets reached $34.5 \pm 6.2\%$ in the HNT group. This value is close to that of the positive control collagen ($31.2\% \pm 3.2\%$), which is markedly higher than that of the control group ($19.3 \pm 5.1\%$). A reversal experiment mediated by tirofiban (GPIIb/IIIa inhibitor) explained the interfacial reactions between platelets and HNTs. As shown in Fig. 2d and 2e, the effect of the HNTs was inhibited by tirofiban (from $34.5\% \pm 6.2\%$ to $15.4\% \pm 4.7\%$), which demonstrates the key role of the GPIIb/IIIa receptor pathway in HNT-induced platelet activation. In conclusion, HNTs cross-link with platelets, causing activation and aggregation to form a primary clot, which triggers the coagulation cascade and forms a stabilized clot.

3.3. Preparation and characterization of HNT-coated hemostatic dressing

There are several forms of hemostatic agents, such as powder, fiber, sponge, and gel, [38] and inorganic-material-coated synthetic fiber dressings have advantages including easy debridement, flexibility,

versatility, simple operation, safety, military shelf-life, and cost-effectiveness. Considering its appropriate mechanical properties and cost, Polyethylene terephthalate (PET) is the fiber substrate used in commercial dressings. Therefore, we developed a PET dressing coated with HNTs (HNTs-PET); a schematic illustration of the preparation is

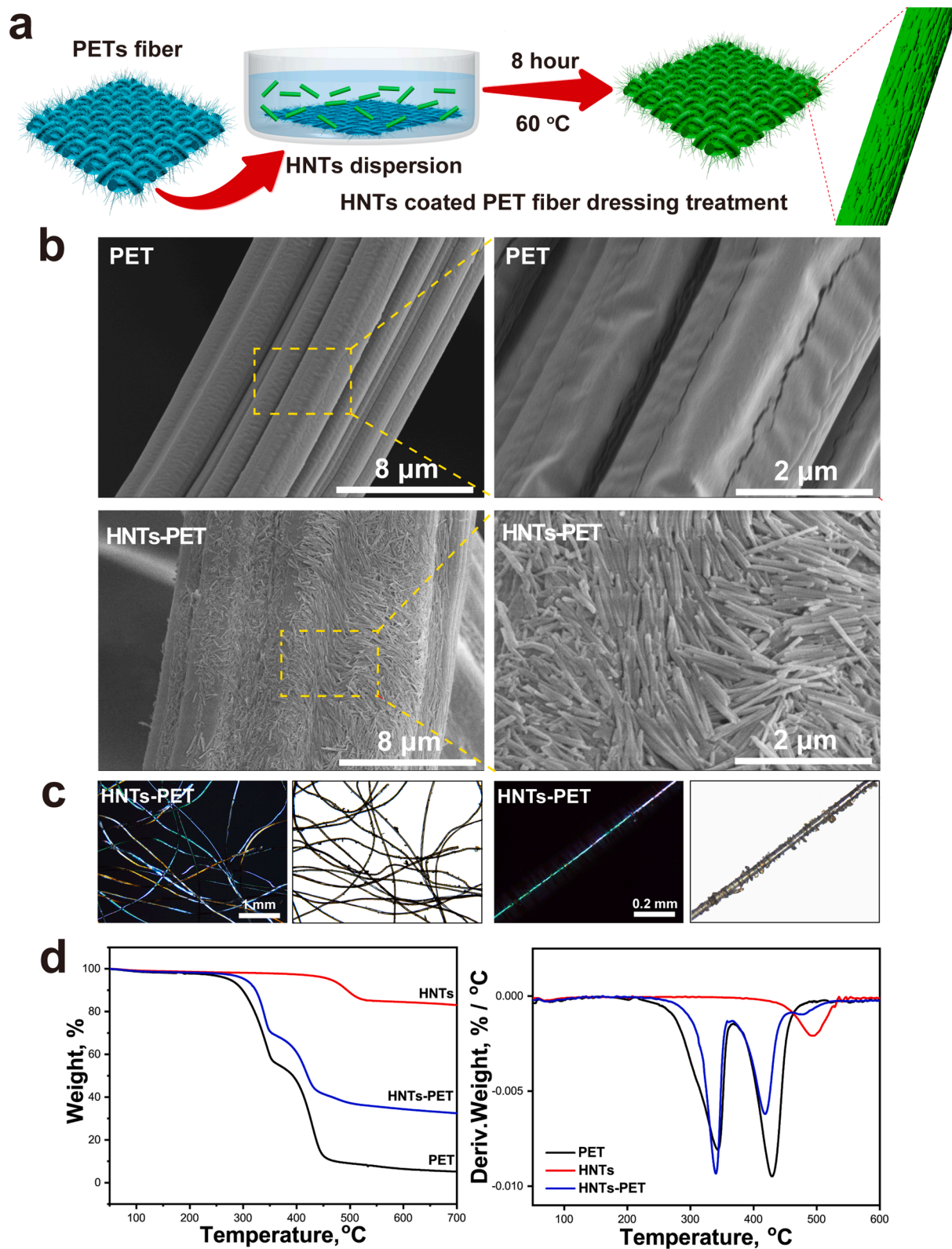


Fig. 3. Characterization of HNTs-PET. (a) Schematic diagram of HNTs-PET preparation. (b) FE-SEM images (c) POM images. (d) TGA curves as well as the derivative weight as a function of temperature.

shown in Fig. 3a.

Physicochemical characterization of HNTs-PET, including XRD and FTIR spectroscopy, suggest the successful anchoring of clay nanoparticles on the fibers (Fig. S4a and S4b). The clotting time results show that the coagulation capacity improves with the increase in HNT content. The 2% HNTs-PET sample achieved the hemostatic effect of the HNT powder (Fig. S4c). Therefore, to balance dispersibility and cost, 2% HNTs-PET was selected for further research (hereafter called HNTs-PET).

The FE-SEM images of HNTs-PET suggest that the rod-shaped HNTs were tightly and evenly distributed on the PET fiber surface (Fig. 3b). In addition, the POM images (Fig. 3c) show the uniform coating of HNTs without changing the fiber structure. In other words, HNTs bind to individual fibers rather than form large aggregates, and the introduction of HNTs does not cause fiber–fiber adhesion. As shown in Fig. 3d, the TGA and derivative thermogravimetry (DTG) curves demonstrate that the HNT loading on the dressing is $\approx 21\%$, which allows high hemostatic efficiency in practical applications. The data also reflect the enhanced thermal stability of HNTs-PET, which allows for its application in high-temperature environments.

3.4. In vitro hemostasis evaluation

For the in vitro clotting test of HNTs-PET, hemoglobin released from free RBCs (not trapped in the clot) was used to indicate the coagulation process (Fig. 4a, left).[39] The absorbance results were normalized to

RHA.[40] It is evident that the RHA level of HNTs-PET drastically decreases, indicating accelerated clotting (Fig. 4a). At 3 min, approximately $68 \pm 4\%$ of the RBCs were trapped in the clot, while this value was $25 \pm 1\%$ and $34 \pm 3\%$ for the control group and PET group, respectively, which confirmed that the coagulant progress was significantly shortened by the HNT coating.

The vascular injury hemorrhage model was further applied to measure the hemostatic capacity of HNTs-PET during massive bleeding emergencies.[40] A hole was opened at the side of a polyethylene hose to imitate the wound on a vessel. HNTs-PET and PET were covered on the hole, and blood containing CaCl_2 was injected into the hose (Fig. 4b). The average blood loss for HNTs-PET is 0.4 ± 0.1 g, which is less than half of the blood loss for PET (1.0 ± 0.1 g), demonstrating that the HNT coating significantly reduces the blood loss (Fig. 4b). Moreover, the blood flow through HNTs-PET slows and has a shorter hemostasis time (Fig. 4c). The HNTs-PET group displayed an average hemostasis time of 96 ± 22 s, which was almost 130 s faster than that of PET (225 ± 35 s). Unlike traditional uncoated dressings that rely on a large amount of fluid absorption to stop bleeding, a small contact interface of HNTs-PET suffices to retard a large volume of blood. The multiple procoagulant interactions of HNTs trigger the immediate formation of primary thrombi when the blood contacts the HNTs-PET interface, blocking the wound and inhibiting blood loss.

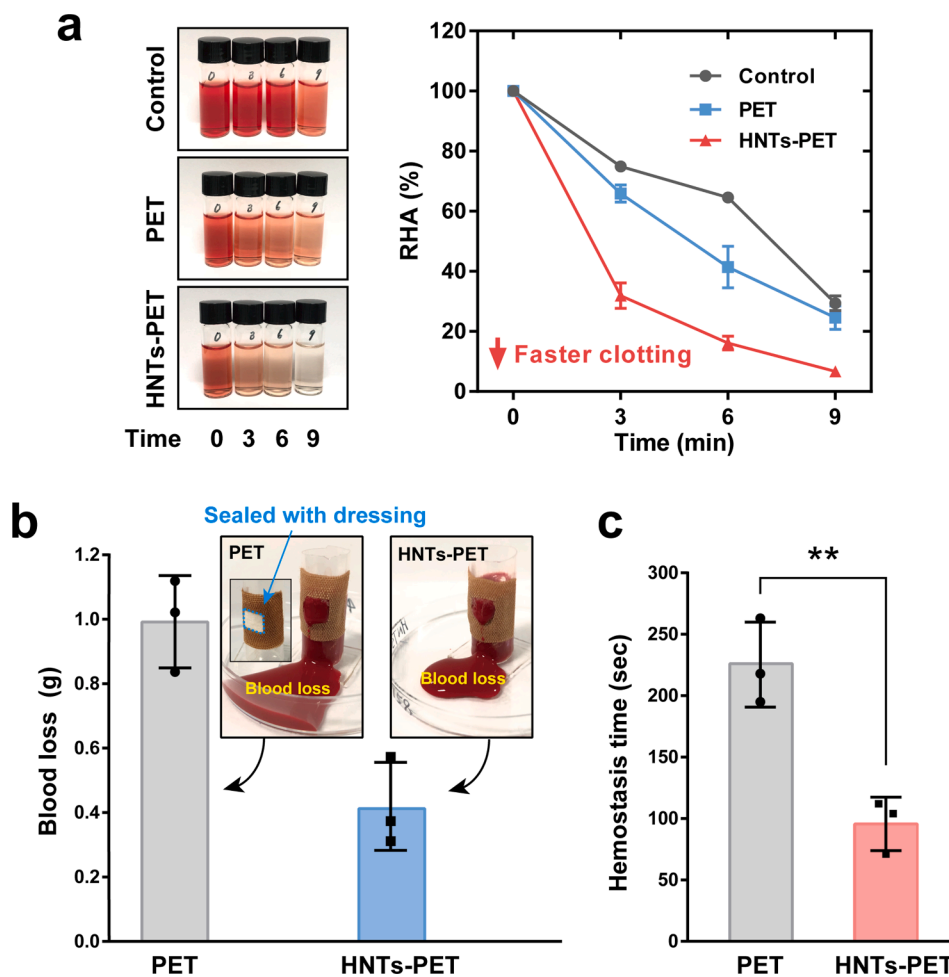


Fig. 4. In vitro hemostatic capacity of HNTs-PET. (a) Representative washing solutions of control, PET, and HNTs-PET at 0, 3, 6, and 9 min (right), which reflect the content of unset RBCs, and the corresponding statistical graph of RHA(t) ($n = 3$) (left). (b) Blood loss and (c) the hemostasis time of HNTs-PET and PET in a vascular injury model. ($n = 3$). (** $p < 0.01$; data were analyzed by student's t-test and are expressed as mean \pm SD).

3.5. Hemorrhage control in animal models

Liver and femoral arteriovenous injury models are widely used for massive hemorrhage hemostasis assays [41–43]. Rupture bleeding in vessel-abundant organs, such as the liver and spleen, is the chief cause of death in clinical or combat situations. In this study, a rat model of heavy liver injury was employed to compare the hemostasis efficacy of HNTs-PET and CG. As shown in Fig. 5a, the clots produced by HNTs-PET and CG can stop the bleeding and close the wound within 3 min, whereas PET failed to completely control the hemorrhage. The hemostasis times of PET, HNTs-PET, and CG were 190 ± 35 s, 138 ± 8 s, and 162 ± 14 s, respectively, suggesting faster hemostasis of the HNT coating (Fig. 5b). Furthermore, HNTs-PET reduced blood loss by more than 70%, making

it remarkably superior to CG (Fig. 5c). Similar to CG, by monitoring the temperature of the wound site, the hemostasis process of HNTs-PET was not accompanied by an exotherm (Fig. 5d).

Subsequently, the femoral artery and vein were severed, resulting in severe bleeding. As shown in Fig. 5e, a large amount of spilled blood in the PET group reflects its limited hemostatic effect, while HNTs-PET and CG can stop bleeding within 3 min. To be precise, the hemostatic time of the HNTs-PET group was 114 ± 30 s, while that of the PET group was 265 ± 57 s (Fig. 5f). Similar to the results of the liver injury model, the amount of blood loss suggests satisfactory hemorrhage control of HNTs-PET and CG (Fig. 5g) in the femoral arteriovenous model without exotherms (Fig. 5h).

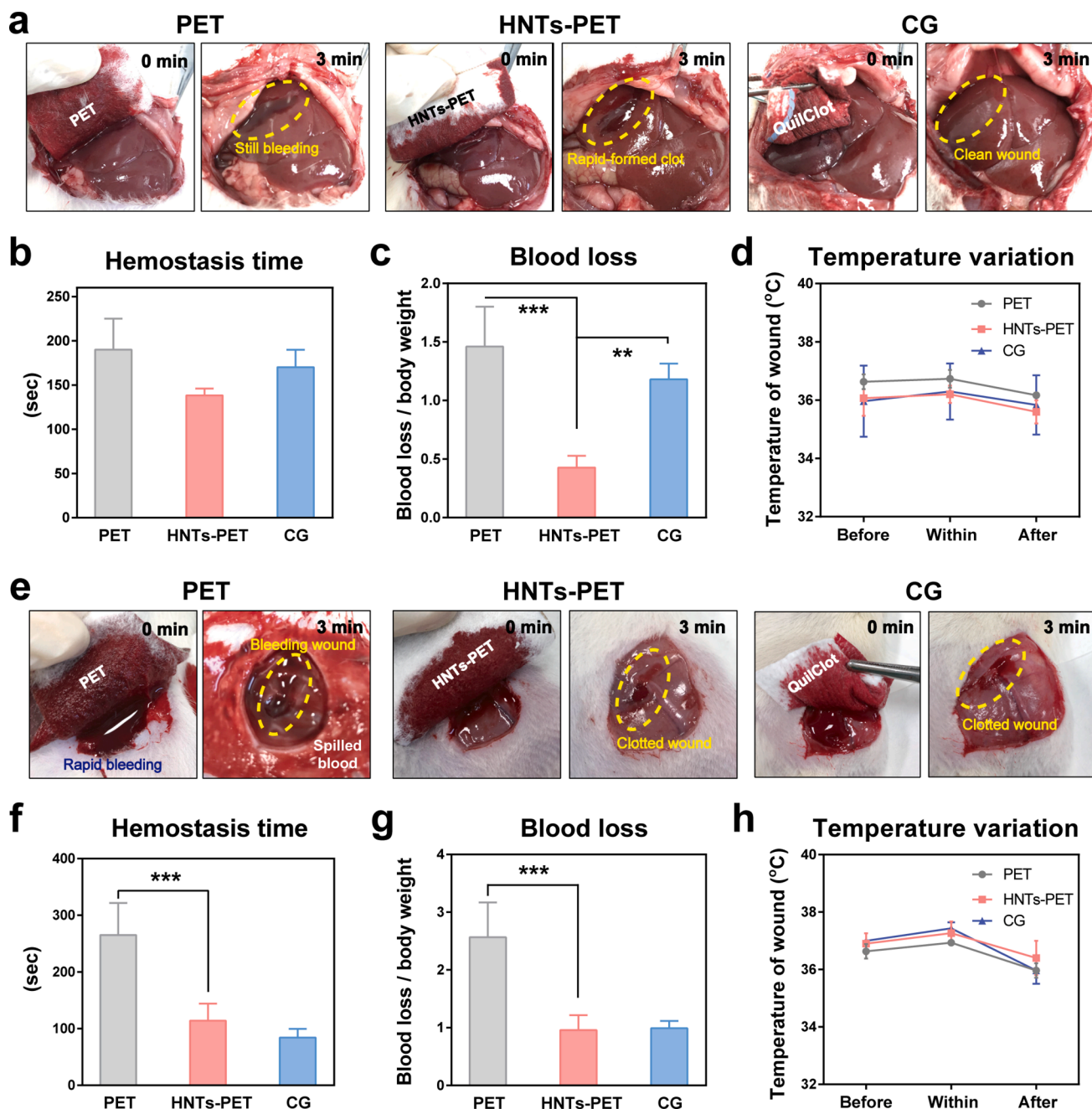


Fig. 5. In vivo hemostatic capability of HNTs-PET in rat liver and femoral arteriovenous injury model. (a) Representative photographs of PET (left), HNTs-PET (middle), and CG (right) in rat liver injury model. The statistics of (b) hemostasis time and (c) blood loss, as well as (d) wound temperature. (e) Representative photographs of PET (left), HNTs-PET (middle), and CG (right) in rat femoral arteriovenous bleeding model. Histograms of (f) hemostasis time, (g) blood loss, and (h) temperature of different groups (** $p < 0.01$, *** $p < 0.001$, and $n = 4$). Data were analyzed by one-way ANOVA and are expressed as mean \pm SD.

3.6. Hemostasis and adhesion resistance of HNTs-PET for skin trauma care

In addition to emergency massive bleeding control, nursing of epidermal trauma is also a crucial issue. The ordinary dressing failed to immediately stop bleeding, which led to frequent replacements and secondary injuries caused by blood clots adhering to the dressing fibers. We created wounds on the skin of the rat back to simulate bleeding from a sharp injury. As shown in Fig. 6a, HNTs-PET and PET were placed on the back of the same rat. Blood continued to infiltrate the PET dressing, but initially only a small amount of blood was absorbed by HNTs-PET (Fig. 6b). The blood stain images show that HNTs-PET significantly reduced blood loss compared to PET (Fig. 6c). As shown in Fig. 6d, the PET-treated wound continued to bleed during the removal process, while the dark red clot closed the wound in the HNTs-PET group, suggesting that the coating of HNTs accelerates clotting and thus avoids continuous bleeding.

The adhesion evaluation of the different dressings was performed at the 2 h mark. After removing the PET dressing, an open wound with a tear caused by adhesion was observed, while the HNTs-PET-treated wound was intact (Fig. 6e). By blotting the wound with tissues (Fig. 6f), exudation was found in the PET-treated wound, but the tissue of the HNTs-PET-treated wound was clear, indicating minimal secondary injury in the latter case. Fig. 6g and 6h show the corresponding quantitative data (blood loss and maximum peel strength, respectively). The blood losses of PET and HNTs-PET group are 38.9 ± 5.9 mg and

19.9 ± 0.8 mg, and the maximum peel strength for the two groups were 38.0 ± 4.9 mN and 19.7 ± 5.1 mN, respectively. In summary, these results confirmed that the HNT coating not only remarkably controlled the sustained bleeding of epidermal wounds but also reduced the adhesion of dressing fibers to wounds. In addition, no significant amount of HNT residue was observed at the wound site, proving the superiority of HNTs-PET over other forms of hemostatic agents, such as powders, gels, and sprays.

3.7. Biocompatibility of HNTs-PET

As shown in Fig. 7a, barely dead skin fibroblast cells (orange-red) were observed in the live/dead stains of the HNTs-PET-treated groups. The CCK-8 data in Fig. 7b also show that the cell viability of each group was higher than 95%, indicating that HNTs-PET was non-cytotoxic. A blood compatibility test (from 37.5 to 1200.0 $\mu\text{g mL}^{-1}$) also revealed low hemolysis of HNTs (Fig. 7c). A previous study also showed that HNTs were compatible with blood in vivo [44]. Next, a skin irritation assay was performed on the rat model. After 24 h, no obvious skin irritation, such as erythema, pruritus, or swelling, was observed (Fig. 7d). Moreover, H&E staining of skin slices demonstrated no inflammatory cell infiltration in both HNTs-PET and PET (Fig. S5), suggesting their non-inflammation in skin contact within 24 h. Based on these results, it can be concluded that HNTs-PET is a safe hemostat with good biocompatibility.

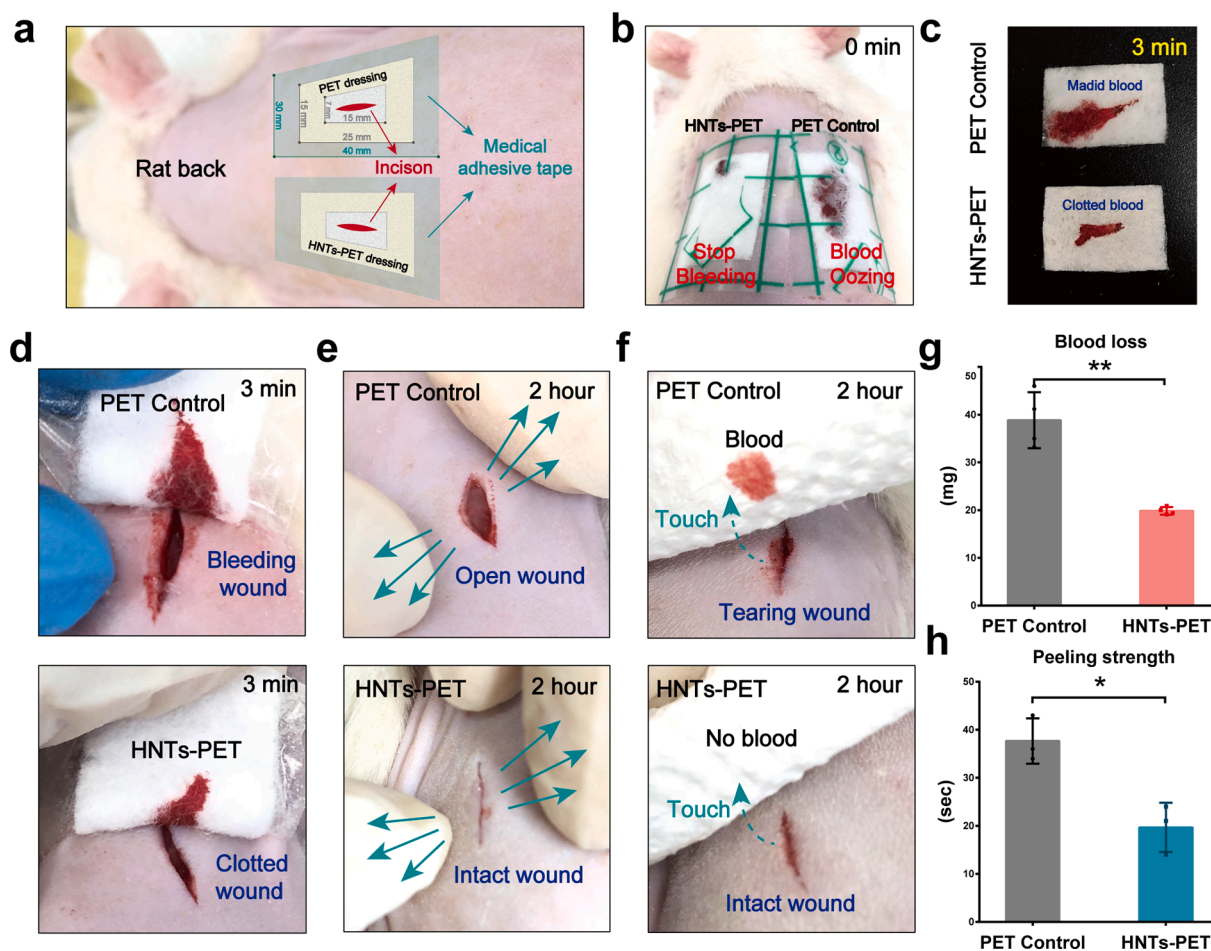


Fig. 6. In vivo hemostatic capability of HNTs-PET in rat back skin injury model. (a) Schematic diagram of two different dressings on the rat back. (b) Photographs of PET and HNTs-PET applied on the wounds at 0 min. (c) Comparison of bleeding between PET and HNTs-PET at 3 min, and photos of wounds at (d) 3 min and (e) 2 h. (f) The secondary bleeding situation. (g) Histogram of blood loss at 3 min. (h) Maximum peeling forces statistics at 2 h (* $p < 0.05$, ** $p < 0.01$, and $n = 4$; data were analyzed by student's t -test and are expressed as mean \pm SD).

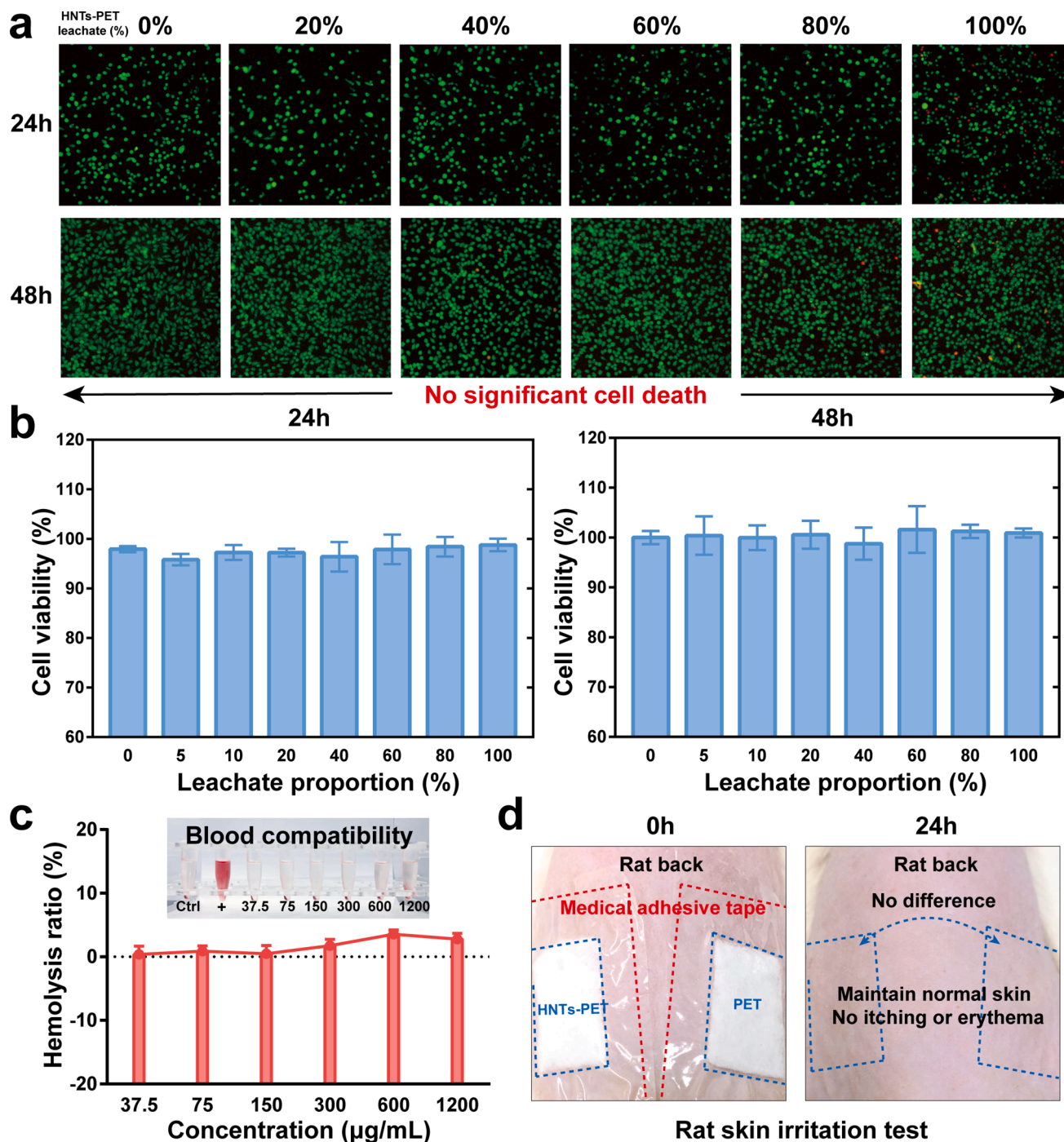


Fig. 7. In vitro and in vivo compatibility test of HNTs-PET. (a) AO/EB live/dead cell staining and (b) cell viability assay ($n = 4$). (c) Blood compatibility (d) Skin irritation study.

4. Discussion

The hemostatic capacity of a material is closely related to its physical structure and surface interface characteristics. The hollow tubular structure of HNTs imparts a large surface area, pore volume, and CEC, and the Si–O–Si groups on the outer surface results in abundant negative charges [17]. These properties make HNTs suitable candidates for use as hemostatic materials. In this study, we confirmed the excellent hemostatic capacity of HNTs and clarified their underlying procoagulant mechanisms (Fig. 8), which are as follows: (i) concentrating blood by absorbing water through their super-hydrophilic surface and porosity of the nanotubes; (ii) interaction of the HNTs' abundant negatively

charged surface with FXII, self-activating into FXIIa and triggering the internal coagulation cascade; and (iii) accelerating clot formation by activating and linking with platelets.

The high water-absorption capacity of HNTs is first correlated with their unique tubular structure, and interlayer water exists in raw halloysite (interlayer spacing is 10 Å). Although the HNTs are used in a dehydrated state (interlayer spacing of 7 Å), water can enter the lumen and interlayer upon contact with aqueous liquids such as blood and body liquid. In addition, the high pore volume ($\approx 0.3\text{--}0.7\text{ cm}^3/\text{g}$) and high aspect ratio of nanotubes also produce capillarity, [45] which is beneficial to water absorption. The results shown in Fig. 1d, 1e, and 1f confirmed the high adsorption ability of HNTs. The water adsorption of

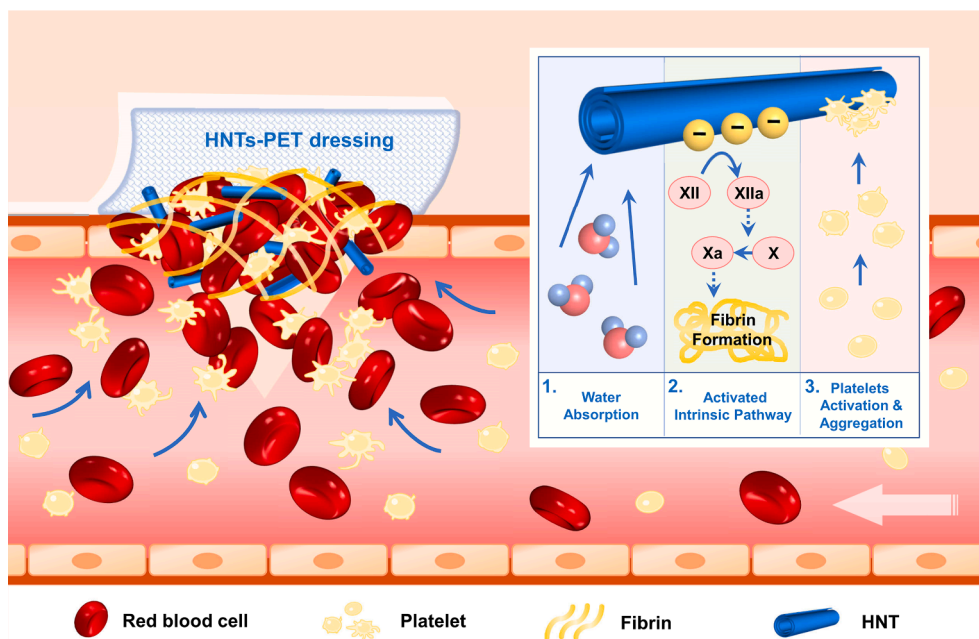


Fig. 8. Schematic depicting the hemostatic mechanisms of HNTs in the bleeding site.

HNTs and zeolite was significantly higher than that of MMT and kaolin (Fig. S2a), and the water in blood plasma quickly interacted with HNTs upon contact, effectively concentrating the blood. The microporosity and CEC of the materials also affect hemostasis. For example, the exchange of Na^+ in blood with Ca^{2+} in the zeolite cage causes the release of Ca^{2+} into the blood [46]. Ca^{2+} (also known as clotting factor IV) is an important cofactor for the activation of factor IX, factor X, prothrombin, and factor XIII, playing a vital role in the coagulation cascade [47]. Unlike lamellar kaolin, all interlayer cations of tubular HNTs are exchangeable, which results in a higher CEC (11 meq/100 g) [45,48]. Combined with the spontaneous coagulation of citrated blood on the HNT table without additional recalcification (Fig. 1f), the unique structure and properties of HNTs clearly lead to the improvement of hemostasis.

The intrinsic coagulation pathway often activated by the contact of blood with negatively charged surfaces, also known as a “contact system,” has been proven as the coagulation mechanism of kaolin [49]. Therefore, the APTT assay, a monitor of intrinsic coagulation, usually uses kaolin as a pathway activator.[27,28] Our study found that the APTT of the HNTs was shorter than that of kaolin (Fig. 2a), and HNTs were the most negatively charged among the inorganic hemostatic clays (Fig. 2b). Therefore, the shorter APTT of HNTs may be ascribed to their richer surface negative charges (zeta potential: $\approx -51.6 \pm 1.6$ mV at pH 7.2). These data confirm the more effective FXII self-activation of HNTs, which is beneficial for acute intrinsic coagulation cascade triggering.[9] In addition, the negative surface charge of materials is also considered to be advantageous for hemostasis via plasma protein adsorption and platelet activation.[50] However, since hemostatic function depends solely on the blood-clotting activity of the hosts, kaolin may be less effective in coagulopathic patients [13]. Our study found that the transformation of the HNT surface charge does not significantly affect the whole blood clotting time (Fig. S2b), suggesting a partial contribution of coagulation cascade activation in HNT hemostasis. This confirms that the clotting acceleration of HNTs is multi-triggered, which is beneficial for bleeding control in coagulopathy that lacks certain clotting factors.

In addition to physical and biochemical actions, platelets play a crucial role in the initial thrombosis of topical hemostatic agents. In general, the conventional wound hemostatic response involves two consecutive pathways [51]. In the preliminary stage, external stimuli

activate platelets through the GPIIb/IIIa complex on their surface; these activated platelets grow pseudopods and aggregate, sticking to the injured area. Then, the coagulation cascade is activated and magnified, and fibrin is generated to trap blood cells and form firmer clots. Tubular materials, such as carbon nanotubes, can interact with platelets, resulting in the depletion of intracellular Ca^{2+} stores, platelet activation, and coagulation [52]. In this work, the platelet activation, aggregation, and initial clot formation triggered by HNTs were investigated using FE-SEM and FCM assays. These effects of HNTs are dependent on the GPIIb/IIIa receptor pathway, which can be suppressed by tirofiban (GPIIb/IIIa receptor antagonist) [29,30]. The large surface area facilitates the sub-micron interaction with platelets and plasma proteins, which is the reason why some microporous nanomaterial interfaces activate platelets [53]. The high aspect ratio, large surface area, and abundant porosity of HNTs facilitate interaction with platelets. In addition, platelet adhesion is generally supported by specific interactions between membrane receptors and plasma proteins adsorbed on the surface of nanomaterials (protein crowns) [54]. Interestingly, we observed that platelets adhered and cross-linked with HNTs (Fig. 2c), which may be related to the adsorption of coagulation-related proteins in plasma on the surface of HNTs through electrostatic interactions [55].

The stability of the hemostasis coating on fiber surfaces is critical for practical applications. The interfacial interactions between HNTs and PET fibers include Van der Waals forces, such as dipole-dipole forces and hydrogen bonds. First, HNTs are polar molecules due to the presence of Si–O–Si groups on the outer surface and Al–OH groups on the inner surfaces [56]. The ester group of PET has a large dipole moment, so it is also polar. Therefore, HNTs and PET experience strong Van der Waals forces. Second, the silanol and aluminol groups of HNTs can interact with the carbonyl groups of PET via hydrogen bonding interactions. The HNT coating on the PET fiber surfaces is stable owing to the interactions by the drying-driven assembly process. The stability of the HNT coating on the fibers was also confirmed in a previous study [57]. In addition to the XRD patterns and FTIR spectra (Fig. S4a and S4b), the SEM and POM results confirmed the anchoring of the nanotube coating on the PET fibers (Fig. 3b and 3c). Negligible nanotubes are peeled off from the fibers during application, which ensures the stability of the hemostatic effect and prevents distal thrombosis and local adverse reactions [58]. The stable HNT-coated PET hemostatic dressing reduced blood loss in the liver injury model by approximately 70% (Fig. 5c), and

the hemostatic time of arteriovenous hemorrhaging was shortened from 265 ± 57 s to 114 ± 30 s (Fig. 5f), without heat release and tissue adhesion (Fig. 5d, 5 h, and 6 h).

Biocompatibility, including cytotoxicity, hemolysis, and skin irritation, is an important safety indicator for the application of hemostatic materials. The fibroblast cell, blood compatibility, and rat skin irritation test revealed high biosafety of the HNT-coated fiber dressing. These results agree with those of previous studies, which demonstrated that HNTs are biocompatible nanomaterials. As expected, no inflammatory cell infiltration was observed in the skin that contacted HNTs-PET in a short time, and mineral-based hemostats were not expected to be left in contact with the body for more than 24 h. Therefore, the safety of the HNTs-PET for up to 24 h could also be guaranteed based on the present and previous studies. In summary, the advantages of the HNT hemostat include its excellent hemostatic performance, flexible product form, low wound adhesion, no exothermic effect, and high biosafety, making it a promising material for effective wound management in clinical applications.

5. Conclusion

In summary, we found that HNTs, as a novel clay hemostatic material, remarkably improve hemostasis via multiple dependent approaches: (i) concentrating blood by absorbing water through their super-hydrophilic surface and tubular structure; (ii) triggering an intrinsic coagulation cascade by negatively charged surface interaction; and (iii) accelerating clot formation by activating and linking with platelets. The multi-triggered clotting of HNTs avoids wound burn caused by heat released in an exothermic reaction, which often occurs for inorganic hemostatic materials. The HNTs-PET dressing prepared by the impregnation method remarkably controls massive hemorrhaging and skin bleeding in animal models. Moreover, HNT-coated fiber surfaces hinder the formation of a tight link between the clot and dressing fiber, thus avoiding wound adhesion. HNT coating also shows excellent biocompatibility, low hemolysis, and no skin irritation. In conclusion, this work provides profound insight into the physical and biological interactions between HNTs and blood from multiple perspectives. The improved hemostatic performance of the HNT-coated dressing—without adhesion and burning—is a promising advancement for hemostatic material development.

Declaration of Competing Interest

The authors declare that they have no known competing financial interests or personal relationships that could have appeared to influence the work reported in this paper.

Acknowledgments

We acknowledge the financial support received from the National Natural Science Foundation China (52073121), Innovation Team Project of Guangdong Provincial Department of Education (2020KCXTD003), Natural Science Foundation of Guangdong Province (2019A1515011509), Local Innovative and Research Teams Project of Guangdong Pearl River Talents Program (grant number 2017BT01Y036) and GDUPS (2019), Science and Technology Planning Project of Guangdong Province (2019A050513004), Science and Technology Program of Guangzhou (202102010117), and Fundamental Research Funds for the Central Universities (21619102).

Appendix A. Supplementary data

Supplementary data to this article can be found online at <https://doi.org/10.1016/j.cej.2021.132049>.

References

- [1] J.T. Howard, R.S. Kotwal, C.A. Stern, J.C. Janak, E.L. Mazuchowski, F.K. Butler, Z. T. Stockinger, B.R. Holcomb, R.C. Bono, D.J. Smith, Use of combat casualty care data to assess the US military trauma system during the Afghanistan and Iraq conflicts, 2001–2017 (vol 154, pg 600, 2019), *JAMA Surg.* 154 (7) (2019) 600, <https://doi.org/10.1001/jamasurg.2019.0151>.
- [2] C. Liu, X. Liu, C. Liu, N. Wang, H. Chen, W. Yao, G. Sun, Q. Song, W. Qiao, A highly efficient, in situ wet-adhesive dextran derivative sponge for rapid hemostasis, *Biomaterials* 205 (2019) 23–37, <https://doi.org/10.1016/j.biomaterials.2019.03.016>.
- [3] X. Yang, W. Liu, N. Li, M. Wang, B. Liang, I. Ullah, A. Luis Neve, Y. Feng, H. Chen, C. Shi, Design and development of polysaccharide hemostatic materials and their hemostatic mechanism, *Biomater. Sci.* 5(12) (2017) 2357–2368, <https://doi.org/10.1039/c7bm00554g>.
- [4] S. Pourshahrestani, E. Zeimaran, I. Djordjevic, N.A. Kadri, M.R. Towler, Inorganic hemostats: The state-of-the-art and recent advances, *Mater. Sci. Eng. C Mater. Biol. Appl.* 58 (2016) 1255–1268, <https://doi.org/10.1016/j.msec.2015.09.008>.
- [5] L.W. Chan, X. Wang, H. Wei, L.D. Pozzo, N.J. White, S.H. Pun, A synthetic fibrin cross-linking polymer for modulating clot properties and inducing hemostasis, *Sci. Transl. Med.* 7 (277) (2015) 277ra29, <https://doi.org/10.1126/scitranslmed.3010383>.
- [6] B.B. Hsu, W. Conway, C.M. Tschabrunn, M. Mehta, M.B. Perez-Cuevas, S.G. Zhang, P.T. Hammond, Clotting mimicry from robust hemostatic bandages based on self-assembling peptides, *ACS Nano* 9 (9) (2015) 9394–9406, <https://doi.org/10.1021/acsnano.5b02374>.
- [7] J. Margolis, The kaolin clotting time; A rapid one-stage method for diagnosis of coagulation defects, *J. Clin. Pathol.* 11 (5) (1958) 406–409, <https://doi.org/10.1136/jcp.11.5.406>.
- [8] J. Lee, H.A. Lee, M. Shin, L.J. Juang, C.J. Kastrup, G.M. Go, H. Lee, Diatom frustule silica exhibits superhydrophilicity and superhemophilicity, *ACS Nano* 14 (4) (2020) 4755–4766, <https://doi.org/10.1021/acsnano.0c00621>.
- [9] R.W. Colman, A.H. Schmaier, Contact system: a vascular biology modulator with anticoagulant, profibrinolytic, antiadhesive, and proinflammatory attributes, *Blood* 90 (10) (1997) 3819–3843, [https://doi.org/10.1016/S0955-3886\(97\)90148-X](https://doi.org/10.1016/S0955-3886(97)90148-X).
- [10] T. Gerlach, J.K. Grayson, K.O. Pichakron, M.J. Sena, S.D. DeMartini, B.Z. Clark, J. S. Estep, D. Zierold, Preliminary study of the effects of smectite granules (WoundStat) on vascular repair and wound healing in a swine survival model, *J. Trauma* 69 (5) (2010) 1203–1209, <https://doi.org/10.1097/TA.0b013e3181c452b5>.
- [11] Tactical combat casualty care guidelines 2 June 2014, *J. Spec. Oper. Med.* 14(3) (2014) 124–131.
- [12] H.H. Murray, Applied clay mineralogy today and tomorrow, *Clay Miner.* 34 (1) (1999) 39–49, <https://doi.org/10.1180/000985599546055>.
- [13] B. Kheirabadi, Evaluation of topical hemostatic agents for combat wound treatment, *US Army Med. Dep. J.* (2011) 25–37.
- [14] M. Long, Y. Zhang, P. Huang, S. Chang, Y. Hu, Q. Yang, L. Mao, H. Yang, Emerging nanoclay composite for effective hemostasis, *Adv. Funct. Mater.* 28 (10) (2018) 1704452, <https://doi.org/10.1002/adfm.201704452>.
- [15] L. Yu, X. Shang, H. Chen, L. Xiao, Y. Zhu, J. Fan, A tightly-bonded and flexible mesoporous zeolite-cotton hybrid hemostat, *Nat. Commun.* 10 (1) (2019) 1932, <https://doi.org/10.1038/s41467-019-09849-9>.
- [16] M.E. Awad, A. Lopez-Galindo, M. Setti, M.M. El-Rahmany, C.V. Iborra, Kaolinite in pharmaceuticals and biomedicine, *Int. J. Pharm.* 533 (1) (2017) 34–48, <https://doi.org/10.1016/j.ijpharm.2017.09.056>.
- [17] Y. Zhao, E. Abdullayev, A. Vasiliev, Y. Lvov, Halloysite nanotubule clay for efficient water purification, *J. Colloid Interface Sci.* 406 (2013) 121–129, <https://doi.org/10.1016/j.jcis.2013.05.072>.
- [18] M.X. Liu, Y. Shen, P. Ao, L.B. Dai, Z.H. Liu, C.R. Zhou, The improvement of hemostatic and wound healing property of chitosan by halloysite nanotubes, *RSC Adv.* 4 (45) (2014) 23540–23553, <https://doi.org/10.1039/c4ra02189d>.
- [19] M. Alavi, A. Totonchi, M.A. Okhovat, M. Motazedian, P. Rezaei, M. Atefi, The effect of a new impregnated gauze containing bentonite and halloysite minerals on blood coagulation and wound healing, *Blood Coagul. Fibrinolysis* 25 (8) (2014) 856–859, <https://doi.org/10.1097/MBC.0000000000000172>.
- [20] R.N. Udangawa, P.E. Mikael, C. Mancinelli, C. Chapman, C.F. Willard, T. J. Simmons, R.J. Linhardt, Novel cellulose-halloysite hemostatic nanocomposite fibers with a dramatic reduction in human plasma coagulation time, *ACS Appl. Mater. Interfaces* 11 (17) (2019) 15447–15456, <https://doi.org/10.1021/acsaami.9b04615>.
- [21] A.C. Santos, I. Pereira, S. Reis, F. Veiga, M. Saleh, Y. Lvov, Biomedical potential of clay nanotube formulations and their toxicity assessment, *Expert Opin. Drug Delivery* 16 (11) (2019) 1169–1182, <https://doi.org/10.1080/17425247.2019.1665020>.
- [22] M. Kryuchkova, A. Danilushkina, Y. Lvov, R. Fakhruddin, Evaluation of toxicity of nanoclays and graphene oxide in vivo: a Parametrium caudatum study, *Environ. Sci.: Nano* 3(2) (2016) 442–452, <https://doi.org/10.1039/c5en00201j>.
- [23] B. Wu, M. Jiang, X. Liu, C. Huang, Z. Gu, Y. Cao, Evaluation of toxicity of halloysite nanotubes and multi-walled carbon nanotubes to endothelial cells in vitro and blood vessels in vivo, *Nanotoxicology* 14 (8) (2020) 1017–1038, <https://doi.org/10.1080/17435390.2020.1780642>.
- [24] Z. Long, Y.P. Wu, H.Y. Gao, J. Zhang, X. Ou, R.R. He, M. Liu, In vitro and in vivo toxicity evaluation of halloysite nanotubes, *J. Mater. Chem. B* 6 (44) (2018) 7204–7216, <https://doi.org/10.1039/c8tb01382a>.

- [25] E.A. Naumenko, I.D. Guryanov, R. Yendluri, Y.M. Lvov, R.F. Fakhrullin, Clay nanotube-biopolymer composite scaffolds for tissue engineering, *Nanoscale* 8 (13) (2016) 7257–7271, <https://doi.org/10.1039/c6nr00641h>.
- [26] H.-Y. Liu, L. Du, Y.-T. Zhao, W.-Q. Tian, In vitro hemocompatibility and cytotoxicity evaluation of halloysite nanotubes for biomedical application, *J. Nanomater.* (2015) 1–9, <https://doi.org/10.1155/2015/685323>.
- [27] E.J. Favalaro, G. Kershaw, S. Mohammed, G. Lippi, how to optimize activated partial thromboplastin time (APTT) testing: Solutions to establishing and verifying normal reference intervals and assessing APTT reagents for sensitivity to heparin, lupus anticoagulant, and clotting factors, *Semin. Thromb. Hemost.* 45 (1) (2019) 22–35, <https://doi.org/10.1055/s-0038-1677018>.
- [28] P. Monagle, *Methods in Molecular Biology, Series Ed., Springer, Berlin, 2013*.
- [29] G.D. Hartman, M.S. Egbertson, W. Halczenko, W.L. Laswell, M.E. Duggan, R.L. Smith, A.M. Naylor, P.D. Manno, R.J. Lynch, G. Zhang, Non-peptide fibrinogen receptor antagonists. 1. Discovery and design of exosite inhibitors, *J. Med. Chem.* 35(24) (1992) 4640–4642, <https://doi.org/10.1021/jm00102a020>.
- [30] Q. Xiang, X. Pang, Z. Liu, G. Yang, W. Tao, Q. Pei, Y. Cui, Progress in the development of antiplatelet agents: Focus on the targeted molecular pathway from bench to clinic, *Pharmacol. Ther.* 203 (2019), 107393, <https://doi.org/10.1016/j.pharmthera.2019.107393>.
- [31] D.J. Li, W. Nie, L. Chen, Y.K. Miao, X. Zhang, F.C. Chen, B. Yu, R.G. Ao, B.Q. Yu, C. L. He, Fabrication of curcumin-loaded mesoporous silica incorporated polyvinyl pyrrolidone nanofibers for rapid hemostasis and antibacterial treatment, *RSC Adv.* 7 (13) (2017) 7973–7982, <https://doi.org/10.1039/c6ra27319j>.
- [32] M. Li, Z. Zhang, Y. Liang, J. He, B. Guo, Multifunctional tissue-adhesive cryogel wound dressing for rapid nonpressing surface hemorrhage and wound repair, *ACS Appl. Mater. Interfaces* 12 (32) (2020) 35856–35872, <https://doi.org/10.1021/acsami.0c08285>.
- [33] Y.S. Zhou, D.Z. Yang, X.M. Chen, Q. Xu, F.M. Lu, J. Nie, Electrospun water-soluble carboxyethyl chitosan/poly(vinyl alcohol) nanofibrous membrane as potential wound dressing for skin regeneration, *Biomacromolecules* 9 (1) (2008) 349–354, <https://doi.org/10.1021/bm7009015>.
- [34] H.L. Fan, L.L. Wang, K.K. Zhao, N. Li, Z.J. Shi, Z.G. Ge, Z.X. Jin, Fabrication, mechanical properties, and biocompatibility of graphene-reinforced chitosan composites, *Biomacromolecules* 11 (9) (2010) 2345–2351, <https://doi.org/10.1021/bm100470q>.
- [35] G. Cavallaro, G. Lazzara, S. Milioto, Exploiting the colloidal stability and solubilization ability of clay nanotubes/ionic surfactant hybrid nanomaterials, *J. Phys. Chem. C* 116 (41) (2012) 21932–21938, <https://doi.org/10.1021/jp307961q>.
- [36] S. Mortazavi, A. Tavasoli, M. Atefi, N. Tanide, N. Radpey, P. Roshan-Shomal, H. Moradi, S. Taeb, CoolClot, a novel hemostatic agent for controlling life-threatening arterial bleeding, *World J. Emerg. Med.* 4 (2) (2013) 123–127, <https://doi.org/10.5847/wjem.j.1920-8642.2013.02.007>.
- [37] S.D. Gordy, P. Rhee, M.A. Schreiber, Military applications of novel hemostatic devices, *Expert Rev. Med. Devices* 8 (1) (2011) 41–47, <https://doi.org/10.1586/erd.10.69>.
- [38] D.A. Hickman, C.L. Pawlowski, U.D.S. Sekhon, J. Marks, A.S. Gupta, Biomaterials and advanced technologies for hemostatic management of bleeding, *Adv. Mater.* 30 (4) (2018) 1700859, <https://doi.org/10.1002/adma.201700859>.
- [39] K. Quan, G. Li, D. Luan, Q. Yuan, L. Tao, X. Wang, Black hemostatic sponge based on facile prepared cross-linked graphene, *Colloids Surf. B. Biointerfaces* 132 (2015) 27–33, <https://doi.org/10.1016/j.colsurfb.2015.04.067>.
- [40] Z. Li, A. Milionis, Y. Zheng, M. Yee, L. Codispoti, F. Tan, D. Poulidakos, C.H. Yap, Superhydrophobic hemostatic nanofiber composites for fast clotting and minimal adhesion, *Nat. Commun.* 10 (1) (2019) 5562, <https://doi.org/10.1038/s41467-019-13512-8>.
- [41] T. Zhu, J. Wu, N. Zhao, C. Cai, Z. Qian, F. Si, H. Luo, J. Guo, X. Lai, L. Shao, Superhydrophobic/Superhydrophilic Janus Fabrics Reducing Blood Loss, *Adv. Healthcare Mater.* 7 (2018), <https://doi.org/10.1002/adhm.201701086>.
- [42] L. Yu, X. Shang, H. Chen, L. Xiao, Y. Zhu, J. Fan, A tightly-bonded and flexible mesoporous zeolite-cotton hybrid hemostat, *Nat. Commun.* 10 (1) (2019) 1–9, <https://doi.org/10.1038/s41467-019-09849-9>.
- [43] A.K. Gaharwar, R.K. Avery, A. Assmann, A. Paul, G.H. McKinley, A. Khademhosseini, B.D. Olsen, Shear-thinning nanocomposite hydrogels for the treatment of hemorrhage, *ACS Nano* 8 (10) (2014) 9833–9842, <https://doi.org/10.1021/nn503719n>.
- [44] J. Zhang, X. Luo, Y. Wu, F. Wu, Y.F. Li, R. He, M. Liu, Rod in Tube: A novel nanoplatform for highly effective chemo-photothermal combination therapy toward breast cancer, *ACS Appl. Mater. Interfaces* 11 (4) (2019) 3690–3703, <https://doi.org/10.1021/acsami.8b17533>.
- [45] A. Glotov, A. Vutolkina, A. Pimerzin, V. Vinokurov, Y. Lvov, Clay nanotube-metal core/shell catalysts for hydroprocesses, *Chem. Soc. Rev.* (2021), <https://doi.org/10.1039/d1cs00502b>.
- [46] J. Li, W. Cao, X. Lv, L. Jiang, Y. Li, W. Li, S. Chen, Zeolite-based hemostat QuikClot releases calcium into blood and promotes blood coagulation in vitro, *Acta Pharmacol. Sin.* 34 (3) (2013) 367–372, <https://doi.org/10.1038/aps.2012.159>.
- [47] E.W. Davie, K. Fujikawa, W. Kisiel, The coagulation cascade: initiation, maintenance, and regulation, *Biochemistry* 30 (43) (1991) 10363–10370, <https://doi.org/10.1021/bi00107a001>.
- [48] W.G. Garrett, Cation-exchange capacity of hydrated halloysite and the formation of halloysite-salt complexes, *Clay Miner.* 4 (22) (1959) 75–80, <https://doi.org/10.1180/claymin.1959.004.22.02>.
- [49] Y. Wu, Contact pathway of coagulation and inflammation, *Thromb. J.* 13 (1) (2015) 1–9, <https://doi.org/10.1186/s12959-015-0048-y>.
- [50] J.V. Edwards, N. Prevost, Thrombin production and human neutrophil elastase sequestration by modified cellulosic dressings and their electrokinetic analysis, *J. Funct. Biomater.* 2 (4) (2011) 391–413, <https://doi.org/10.3390/jfb2040391>.
- [51] M.H. Periyah, A.S. Halim, A.Z. Mat Saad, Mechanism action of platelets and crucial blood coagulation pathways in hemostasis, *Int. J. Hematol. Oncol Stem Cell Res.* 11 (4) (2017) 319–327.
- [52] S.H. Lacerda, J. Semberova, K. Holada, O. Simakova, S.D. Hudson, J. Simak, Carbon nanotubes activate store-operated calcium entry in human blood platelets, *ACS Nano* 5 (7) (2011) 5808–5813, <https://doi.org/10.1021/nn2015369>.
- [53] Z. Chen, F. Li, C. Liu, J. Guan, X. Hu, G. Du, X. Yao, J. Wu, F. Tian, Blood clot initiation by mesoporous silica nanoparticles: dependence on pore size or particle size? *J. Mater. Chem. B* 4 (44) (2016) 7146–7154, <https://doi.org/10.1039/c6tb01946c>.
- [54] X. Shang, H. Chen, V. Castagnola, K. Liu, L. Boselli, V. Petseva, L. Yu, L. Xiao, M. He, F. Wang, K.A. Dawson, J. Fan, Unusual zymogen activation patterns in the protein corona of Ca-zeolites, *Nat. Catal.* 4 (7) (2021) 607–614, <https://doi.org/10.1038/s41929-021-00654-6>.
- [55] M.P. Monopoli, D. Walczyk, A. Campbell, G. Elia, I. Lynch, F.B. Bombelli, K. A. Dawson, Physical-chemical aspects of protein corona: relevance to in vitro and in vivo biological impacts of nanoparticles, *J. Am. Chem. Soc.* 133 (8) (2011) 2525–2534, <https://doi.org/10.1021/ja107583h>.
- [56] P. Yuan, D.Y. Tan, F. Annabi-Bergaya, Properties and applications of halloysite nanotubes: Recent research advances and future prospects, *Appl. Clay Sci.* 112 (2015) 75–93, <https://doi.org/10.1016/j.clay.2015.05.001>.
- [57] A. Panchal, G. Fakhrullina, R. Fakhrullin, Y. Lvov, Self-assembly of clay nanotubes on hair surface for medical and cosmetic formulations, *Nanoscale* 10 (38) (2018) 18205–18216, <https://doi.org/10.1039/c8nr05949g>.
- [58] A.B. Zimrin, Y. Bai, J.B. Holcomb, J.R. Hess, 40 - Hemorrhage control and thrombosis following severe injury, in: C.S. Kitchens, C.M. Kessler, B.A. Konkle, M. B. Streiff, D.A. Garcia (Eds.), *Consultative Hemostasis and Thrombosis (Fourth Edition)*, Elsevier, Philadelphia, 2019, pp. 811–818.

Supplementary Information for

Systematic Studies on Blood Coagulation Mechanisms of Halloysite

Nanotubes-Coated PET Dressing as Superior Topical Hemostatic Agent

Yue Feng^a, Xiang Luo^b, Fan Wu^a, Hongzhong Liu^a, Enyu Liang^c, Rong-Rong He^{b}, Mingxian Liu^{a*}*

^aDepartment of Materials Science and Engineering, ^b College of Pharmacy, Jinan University, Guangzhou 510632, China

^cDepartment of Laboratory Medicine, the Second Affiliated Hospital of Guangzhou University of Chinese Medicine, Guangzhou, 510120, China.

*Corresponding author: Rong-Rong He, Tel: 020-85220850, Email: rongronghe@jnu.edu.cn;
Mingxian Liu, Tel: 020-85222247 Email: liumx@jnu.edu.cn

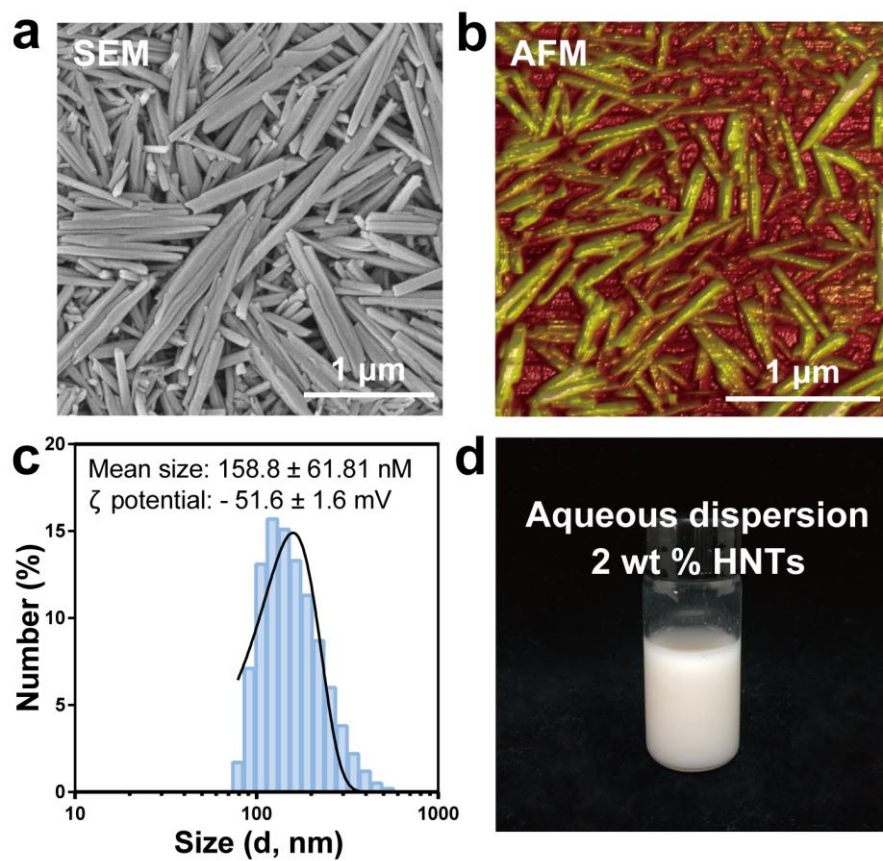


Figure S1. Characterization of HNTs. (a) SEM and (b) AFM images of HNTs. (c) The particle size distribution and zeta potential of HNTs. (d) The photograph of 2 wt% HNTs water dispersion.

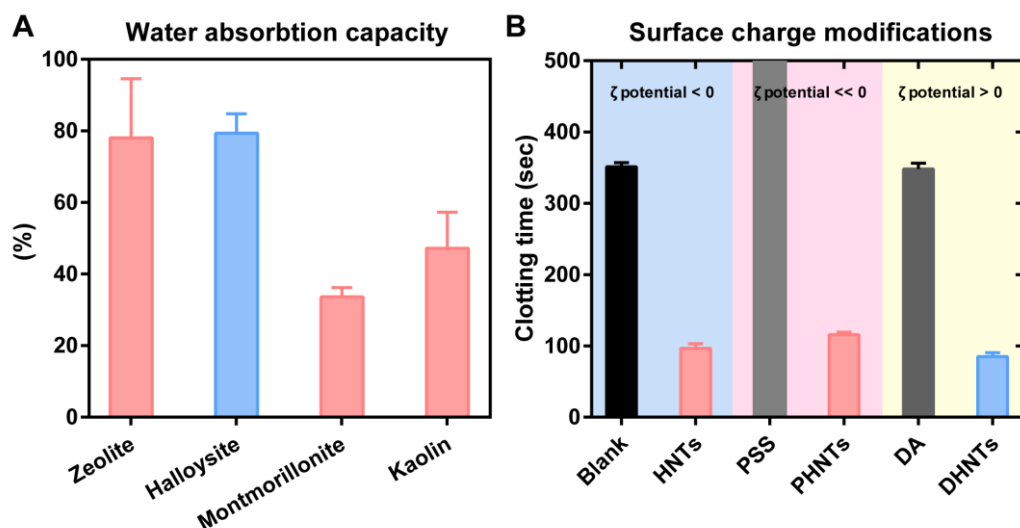


Figure S2. (a) Water absorption capacity of HNTs comparing to other inorganic hemostatic materials. (b) Clotting time of HNTs after surface modifications. Background-color: blue (unmodified, natural HNTs are negatively charged), pink (sodium polystyrene sulfonate modified HNTs have enhanced electronegativity), yellow (dopamine modified HNTs are positively charged).

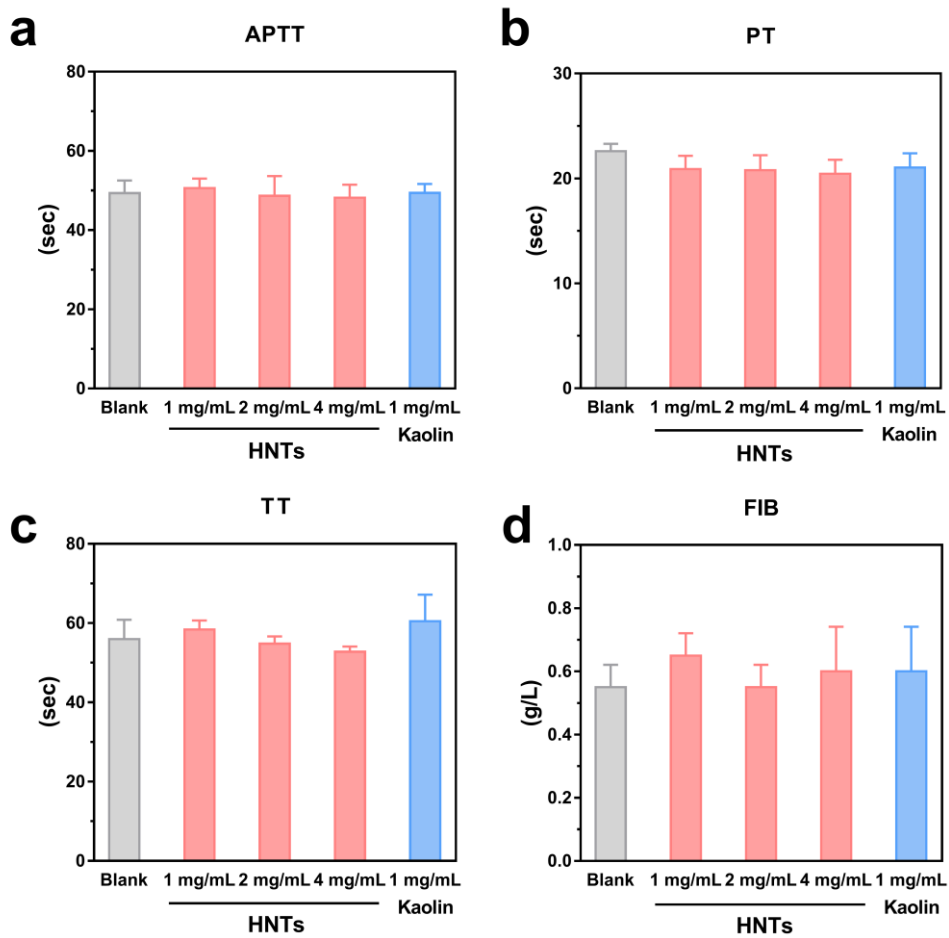


Figure S3. Effect of HNTs or kaolin on clinical coagulation detection. (a) Activated partial thromboplastin time (APTT); (b) prothrombin time (PT); (b) thrombin time (TT), and (c) fibrinogen (FIB) results.

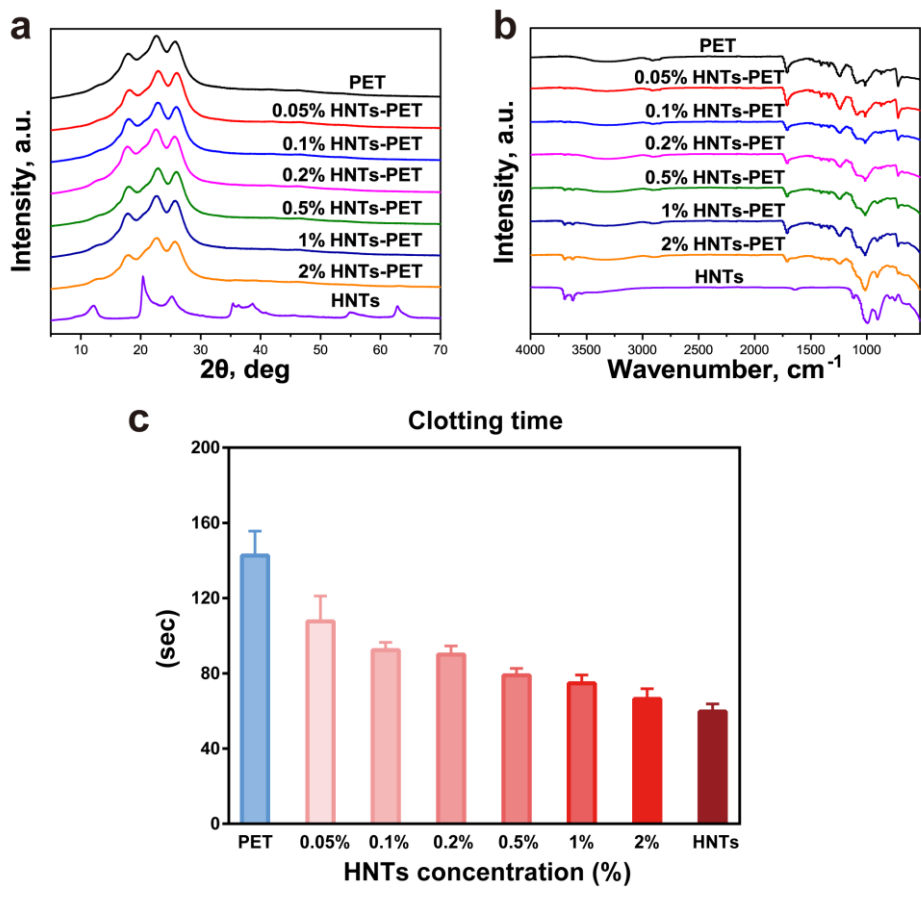
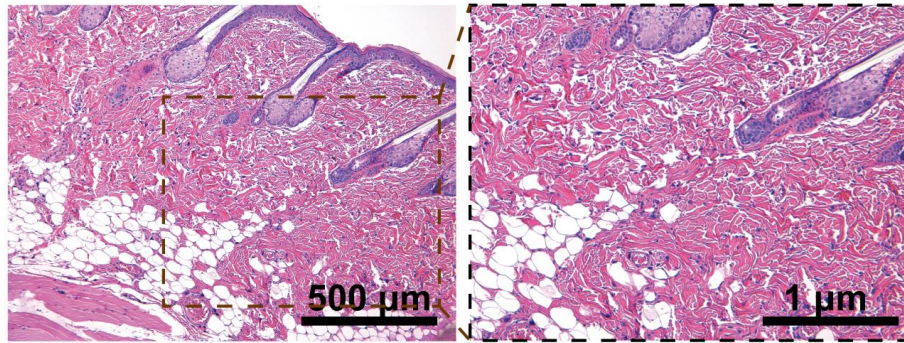
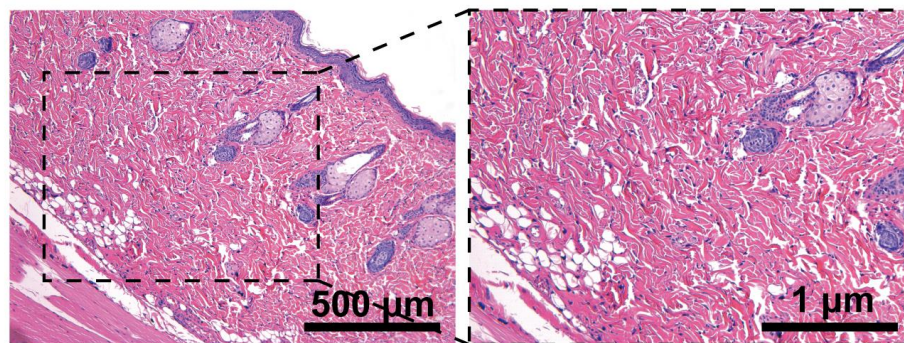


Figure S4. (a) XRD patterns and (b) FTIR spectra, and (c) clotting time of HNTs, PET and different concentrations of HNTs-PET.



PET control skin



HNTs-PET skin

Figure S5. H&E staining of skin sections after 24 h of PET or HNTs-PET exposure.